Remote Sensing of Environment 342 (2026) 115459

Contents lists available at ScienceDirect

Remote Sensing of Environment

journal homepage: www.elsevier.com/locate/rse

Assessment of EnMAP data quality through global product validation activities

Maximilian Brell [a], Philipp Reiners [a,*], Luis Guanter [b], Karl Segl [a], Sabine Chabrillat [a,c], Daniel Scheffler [a], Mariana A. Soppa [d], Niklas Bohn [a,e], Javier Gorrono [b], Alexander Kokhanovsky [a,f], Astrid Bracher [d,g], Martin Bachmann [h], Miguel Pato [h], Mathias Schneider [h], Raquel de los Reyes [h], Maximilian Langheinrich [h], Stefanie Holzwarth [h], Emiliano Carmona [h], Tobias Storch [h], Nicole Pinnel [h], Martin Habermeyer [h], Raymond Kokaly [i], Cindy Ong [j], Robert O. Green [e], Jose Moreno [k], Ferran Gascon [l], Tobias Hank [m], Eyal Ben-Dor [n], Biagio Di Mauro [o], Roberto Colombo [p], Robert Milewski [a], Benjamin Brede [a], Thomas Schmid [q], Cody Anderson [i], Anke Schickling [r], Vera Krieger [r], Michael Bock [r], Laura La Porta [r], Sebastian Fischer [r]

[a] *GFZ Helmholtz Center for Geosciences, Potsdam, Germany*
[b] *Universitat Politecnica de Valencia, Research Institute of Water and Environmental, Engineering (IIAMA), Valencia, Spain*
[c] *Leibniz University Hannover, Institute of Earth System Science, Soil science, Hannover, Germany*
[d] *Alfred Wegener Institute (AWI), Helmholtz Centre for Polar and Marine Research, Bremerhaven, Germany*
[e] *Jet Propulsion Laboratory, California Institute of Technology, Pasadena, CA, USA*
[f] *Philipps University Marburg, Department of Geography, Marburg, Germany*
[g] *University of Bremen, Institute of Environmental Physics (IUP), Bremen, Germany*
[h] *German Aerospace Center (DLR), Earth Observation Center (EOC), Weßling, Germany*
[i] *U.S. Geological Survey (USGS), Geology, Geophysics, and Geochemistry Science, Center, Lakewood, CO, USA*
[j] *Commonwealth Scientific and Industrial Research Organisation (CSIRO), Bentley, WA, Australia*
[k] *Universitat de Valencia, Faculty of Physics, Department of Earth Physics and Thermodynamics, Valencia, Spain*
[l] *European Space Agency (ESA), Frascati, Italy*
[m] *Ludwig-Maximilians-University Munich, Department of Geography, Munich, Germany*
[n] *Tel Aviv University, Department of Geophysics, Tel Aviv, Israel*
[o] *Institute of Polar Sciences, National Research Council, Milan, Italy*
[p] *Earth and Environmental Sciences Department, University of Milano-Bicocca, Milan, Italy*
[q] *Department of Environment, Centro de Investigaciones Energeticas, Medioambientes y Tecnologicas (CIEMAT), Madrid, Spain*
[r] *German Aerospace Center (DLR), Space Agency, Bonn, Germany*

ARTICLE INFO

Keywords:
EnMAP
Imaging spectroscopy
Satellite mission

ABSTRACT

The EnMAP (Environmental Mapping and Analysis Program) satellite, launched on 1 April 2022, is designed to provide high-resolution imaging spectroscopy data for environmental monitoring, resource management and land use mapping. The integrity and quality of the official data products are assessed by the mission's external

* Corresponding author.
E-mail addresses: maximilian.brell@gmail.com (M. Brell), philipp.reiners@gfz.de (P. Reiners), lguanter@fis.upv.es (L. Guanter), segl@gfz.de (K. Segl), chabri@gfz.de (S. Chabrillat), daniel.scheffler@gfz.de (D. Scheffler), Mariana.Altenburg.Soppa@awi.de (M.A. Soppa), urs.n.bohn@jpl.nasa.gov (N. Bohn), xavi.gorronyo@gmail.com (J. Gorrono), kokhanoa@staff.uni-marburg.de (A. Kokhanovsky), Astrid.Bracher@awi.de (A. Bracher), martin.bachmann@dlr.de (M. Bachmann), Miguel.FigueiredoVazPato@dlr.de (M. Pato), Mathias.Schneider@dlr.de (M. Schneider), Raquel.delosReyes@dlr.de (R. de los Reyes), maximilian.langheinrich@dlr.de (M. Langheinrich), stefanie.holzwarth@lbv.de (S. Holzwarth), Emiliano.Carmona@dlr.de (E. Carmona), Tobias.Storch@dlr.de (T. Storch), Nicole.Pinnel@dlr.de (N. Pinnel), martin.habermeyer@dlr.de (M. Habermeyer), raymond@usgs.gov (R. Kokaly), cindy.ong@csiro.au (C. Ong), robert.o.green@jpl.nasa.gov (R.O. Green), jose.moreno@uv.es (J. Moreno), ferran.gascon@esa.int (F. Gascon), tobias.hank@lmu.de (T. Hank), bendor@tauex.tau.ac.il (E. Ben-Dor), biagio.dimauro@cnr.it (B. Di Mauro), roberto.colombo@unimib.it (R. Colombo), milewski@gfz-potsdam.de (R. Milewski), benjamin.brede@gfz.de (B. Brede), thomas.schmid@ciemat.es (T. Schmid), chanderson@usgs.gov (C. Anderson), Anke.Schickling@esa.int (A. Schickling), vera.krieger@dlr.de (V. Krieger), michael.bock@dlr.de (M. Bock), Laura.LaPorta@dlr.de (L. La Porta), sebastian.fischer@dlr.de (S. Fischer).

https://doi.org/10.1016/j.rse.2026.115459
Received 22 July 2024; Received in revised form 24 April 2026; Accepted 25 April 2026
Available online 5 May 2026

Data quality assessment
Validation
CAL/VAL

product validation activities, which are independent of the calibration/validation activities from the ground segment.The external validation is intended to assess, monitor, and report the quality of the L1B (top-of-atmosphere radiance in sensor coordinates), L1C (top-of-atmosphere radiance in map coordinates), and L2A (surface reflectance in map coordinates) user products. This work presents an overview of the EnMAP product validation activities during the commissioning phase and the first two years of the operational phase. Radiometric, spectral, geometric, and general uniformity aspects are evaluated with scene-based analysis methods and through comparison with ground-based reference methods. We find that EnMAP's radiometric calibration is $< 5\%$, both smile and keystone are $< 20\%$ of a pixel, and the Bottom-Of-Atmosphere (BOA) reflectance and Normalized Water-Leaving reflectance are well inside the mission requirements. These results confirm that the EnMAP products fulfill the mission requirements and pave the way for the scientific exploitation and use of the EnMAP products for land, water, and atmospheric applications.

1. Introduction

The satellite imaging spectroscopy mission EnMAP (Environmental Mapping and Analysis Program) maps the Earth's surface in 224 spectral bands with high spatial and spectral resolution (Storch et al., 2023; Guanter et al., 2015). EnMAP was launched on 1st April, 2022, passed the seven-month commissioning phase (CP) successfully, and has been in the operational phase (OP) for 3 years now. The OP is scheduled to run until at least 2027. The primary goal of EnMAP is to provide analytically and quantitatively interpretable hyperspectral data for a wide range of applications distributed globally (Guanter et al., 2015). Application fields of environment and resources are covered (Chabrillat et al., 2024), such as land use and land cover mapping, vegetation (Hank et al., 2019), soil properties (Chabrillat et al., 2019; Chabrillat et al., 2023), water quality monitoring (Giardino et al., 2019; Soppa et al., 2022), aerosol optical depth (Laffoy et al., 2025) and mineral exploration (Asadzadeh and Chabrillat, 2025). The quantification of snow parameters (Kokhanovsky et al., 2026), nighttime lights (Bachmann and Storch, 2023) and methane plumes (Roger et al., 2024) underline the potential and relevance of the mission and the scientific requirements regarding the provided data quality.

To serve the different applications with quantifiable and analytical hyperspectral Earth Observation (EO) data across the operational lifetime, it is crucial to verify and monitor EnMAP's data quality. This process is essential to interpret and contextualize derived products, analysis, and results. It lays the foundation for the transferability and generalizability of the EO measurements. The overall data quality and suitability for analytical interpretation depends on the comprehensive interaction of radiometric, geometric, and spectral data quality and the performed compensation of atmospheric influences (Thompson et al., 2020; Guanter et al., 2006).

To ensure adequate EnMAP data quality and accuracy, the mission provides validation activities and assessments independent from the official calibration and quality control efforts of the Ground Segment (GS) at the DLR Earth Observation Center (EOC). These validation activities are conducted by the EnMAP Science and User Segment, represented by the GFZ Helmholtz Center for Geosciences, supported by the AWI Alfred-Wegener-Institute Helmholtz Center for Polar and Marine Research for the validation over water, during CP and OP (Brell et al., 2021; Chabrillat et al., 2022). The objective of the independent product validation activities, which will cover the whole operational lifetime, is to evaluate and monitor the quality of EnMAP data provided to the users holistically and from scientific user perspectives. As the findings are considered to optimize the calibration and preprocessing, they support and guarantee the transferability and generalizability of the EO measurement. Opposed to the mission-internal pre-flight and onboard calibration data used in the GS's monitoring and quality control tests, the independent validation only relies on the EO data (image-based) and, for specific scenarios, on field measurements (in-situ-based). Several hyperspectral data quality assessment methods and scenarios are realized independently to evaluate the accuracy, precision, consistency, and reliability of hyperspectral EnMAP data products.

The main objective of this paper is to introduce the EnMAP quality assessment framework and to present the status and results of the quality assessment activities for the main data products in the first years of the EnMAP mission. The versatile set of validation scenarios, activities, procedures, and methods to validate each EnMAP product are described in detail. Quantitative results of the validated parameter performance are confronted with the mission and user requirements. The paper is organized as follows: the general overview, including the EO validation frameworks, relevant EnMAP sensor and orbit specifications, data products, and mission requirements are given in the remaining introduction to place the independent validation efforts in the proper context. Section 2 describes the EnMAP data products and in-situ measurements that are used. Section 3 outlines the scientific background and methodology of the EnMAP validation tasks, while Section 4 presents the corresponding results. Section 5 discusses and summarizes the main findings and conclusions of the article.

1.1. EnMAP validation framework

Validation is the process of accessing the on-orbit quality of the hyperspectral data products with independent reference data (Loew et al., 2017; CEOS, 2023; Justice et al., 2000; Niro et al., 2021). The validation framework of EnMAP focuses on the overall radiometric, geometric, reflective, and spectral data quality. An application-driven validation of secondary bio-geophysical products derived from the atmospherically-corrected data is not being included as it is out of scope of this validation approach due to the various applications of hyperspectral data. Various comparable hyperspectral missions have adopted and customized calibration and validation frameworks (Thompson et al., 2023; Coleman et al., 2024; Turpie et al., 2023; Cogliati et al., 2021; Czapla-Myers et al., 2016; Green et al., 2003; Alonso et al., 2019) which are similar in principle to multispectral validation frameworks (Gascon et al., 2017; Haque et al., 2023). Every EnMAP measurement has inherent systematic and random error contributions. Despite extensive pre-flight and in-flight (on-board, sun, and moon) calibration and quality efforts (Storch et al., 2023), these errors are significantly reduced but cannot be entirely excluded. In this study, the focus is to monitor the impact of calibration efforts and instrument stability and, thus, the compliance of mission requirements from the user perspective.

The overall framework developed for this purpose is called “EnVAL”. Fig. 1 overviews the performed validation scenarios and investigated parameters. The respective products and parameters are checked intensively and regularly during the CP and OP following the guidelines given by the Product Validation Plan (PVP) (Guanter et al., 2022). For the image-based validation scenarios, scene properties suitable for a specific validation scenario in terms of, e.g., spatial or spectral homogeneity or contrast, atmospheric influences were determined. As the mission progresses, it is planned to increase the representativeness and transform the validation activities into a holistic and well-balanced quality monitoring framework.

1.2. EnMAP sensor and orbit specification

EnMAP covers a spectral range from 418.2 nm to 993.0 nm (VNIR) and 902.2 nm to 2445.5 nm (SWIR) with a prism-based dual spectrometer design. The VNIR spectral range is covered with an average spectral sampling distance (SSD) of 6.4 nm and full width half maximum (FWHM) of 7.8 nm over 91 bands. The SWIR has an average SSD of 10.0 nm and an FWHM of 9.5 nm over 133 transferred and delivered bands. 22 bands in the SWIR, influenced by a strong atmospheric absorption, are not transferred. Fig. 2 shows the VNIR-SWIR wavelength coverage, including the overlap based on the relation between SSD and FWHM. A signal-to-noise ratio (SNR) of 620:1 at 495 nm and 230:1 at 2200 nm is achieved related to a reference radiance level of 30% surface albedo, 30 deg. Sun zenith angle, at ground sea level, and 40 visibility with rural atmosphere (Storch et al., 2023). For the VNIR sensor, the low gain mode is entered for signals that exceed a certain threshold level. For the SWIR sensor, all bands below 1980 nm are set to low gain, and bands above 1980 nm are set to high gain mode. The curved prism design minimizes smile and keystone and thus maximizes spectral and spatial uniformity. Onboard calibration through sun diffuser and calibration spheres for linearity and doped Spectralon for spectral calibration ensures radiometric and spectral consistency and stability. The 1000 across-track pixel detectors in combination with an instantaneous field-of-view of 9.5 arcsec result in a ground sampling distance (GSD) of 30 m × 30 m and a swath width of 30 km. A direct pointing accuracy of ≈55 m is achieved, which is improved to ≈20 m based on image matching to a reference. In 27 days, 398 polar, sun-synchronous orbits are performed at a mean altitude of 642 km. The target revisiting time of 27 days can be reduced to 4 days in the acquisition user request due to the across-track off-nadir pointing capability of ±30° in case the challenges regarding the analytical interpretation arising from off-nadir acquisitions are accepted. The maximum length of a single acquisition (along-track) is limited to ≈990 km, and the daily maximal capacity is 5550 km. Further details on the design of the EnMAP sensor and mission can be found in (Kaufmann et al., 2015).

1.3. EnMAP mission requirements

The mission requirements have been set for significant quality parameters that must be met during the mission (Guanter et al., 2015). These parameters include radiometric, spectral, reflectivity, geometric, and general uniformity requirements, particularly relevant to the end users. Table 3 in section 5.1 overviews the relevant requirements investigated in this study.

1.4. EnMAP product description

A detailed description of the provided EnMAP products and their processing can be found in Storch et al., 2023; Bachmann et al., 2021), and the full Product Specifications and technical details in the ATBDs are available at https://www.enmap.org (DLR, 2025). In brief, after a successful EO acquisition, the datatake is cut into 30 km × 30 km tiles, and processed to the three primary processing levels (Level 1B, Level 1C, and Level 2 A). During this processing, per-pixel quality layers and rich metadata is generated, including geolocation information (as RPMs), geolocation accuracy with respect to independent control points, and information on the atmospheric conditions. This information is then attached to the L0 product, only which is then archived. Thus when ordering a L1B, L1C or L2A product, the archived L0 data is re-processed on demand, guaranteeing the usage of the latest processor version and calibration information.

The L1B product contains radiometrically corrected and spectrally characterized Top-Of-Atmosphere (TOA) radiance data in sensor geometry, provided separately for VNIR and SWIR. The L1C product represents orthorectified TOA radiance (L_{TOA}) data stacked into a single data cube and projected to user-selectable coordinate systems with 30 m pixel size. For geometric correction, a direct georeferencing procedure is applied using the Copernicus DEM (ESA and Airbus, 2022) and if available, Sentinel-2 (ESA, 2018) derived Ground Control Points (GCPs)

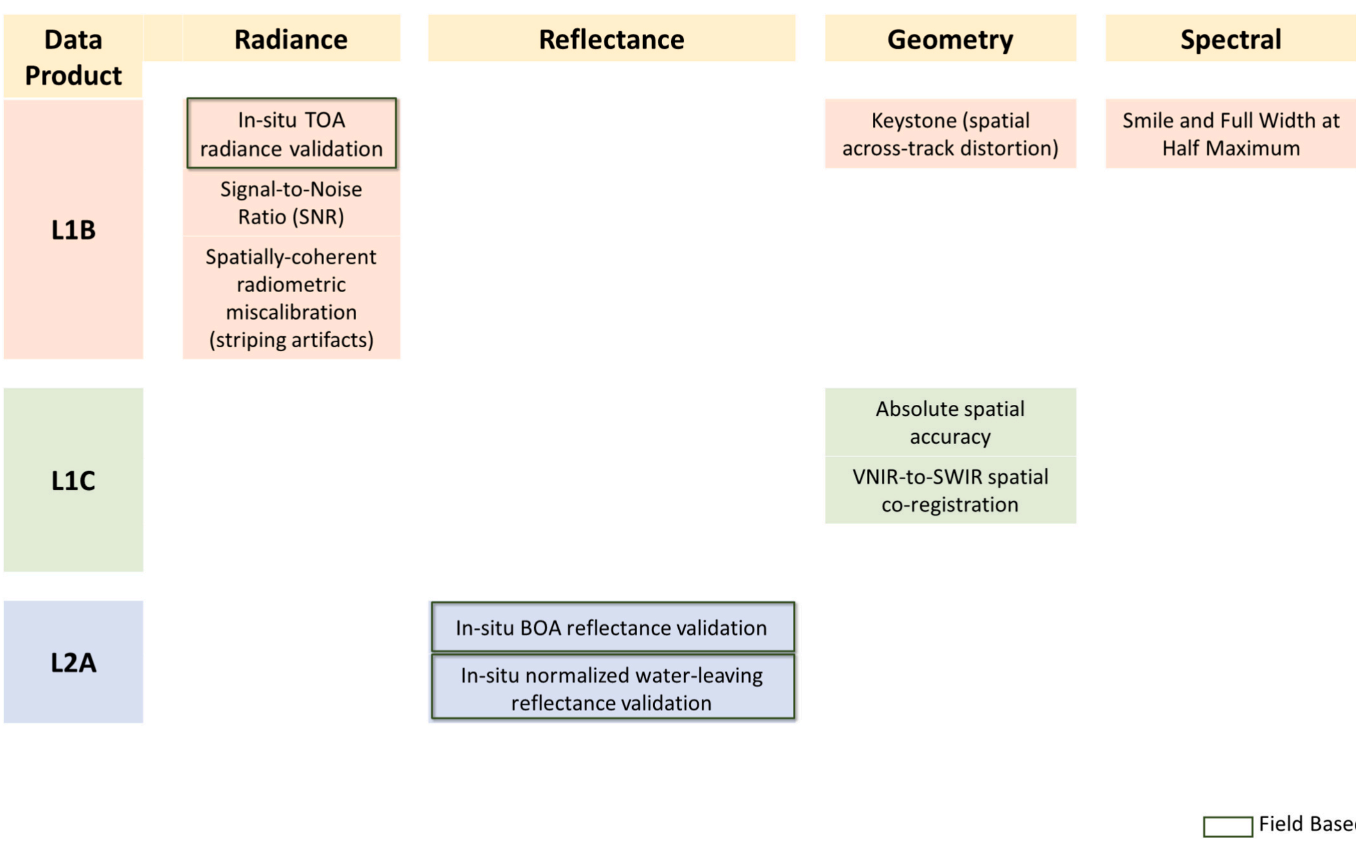

Fig. 1. Overview of the various validation scenarios, the corresponding quality parameters, and the EnMAP product levels.

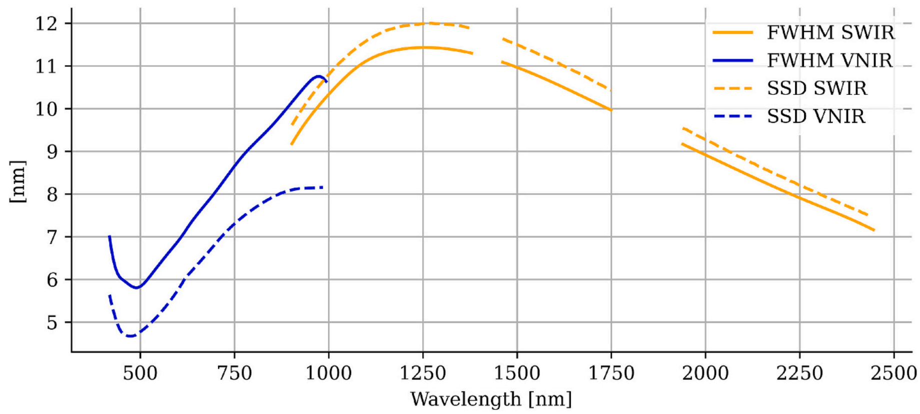

Fig. 2. Relation between SSD and FWHM for the EnMAP VNIR and SWIR sensors.

to optimize intrinsic and extrinsic pointing parameters. The L2 A product provides atmospherically corrected Bottom-Of-Atmosphere (BOA) surface reflectance using the Python-based Atmospheric Correction (PACO) (de los Reyes et al., 2020) and Modular Inversion Processor (MIP) (Heege et al., 2014; Kiselev et al., 2015) processors for land and water surfaces, respectively. Both processors are considering the adjacency effect, and the L2 A "Surface Reflectance (land)" product can also include a compensation for terrain illumination effects as well as haze and cirrus, and is certified as CEOS Analysis Ready Data ((CEOS, 2025)). All data products including metadata and per-pixel quality layers are provided freely to registered users via the EOWEB® GeoPortal (DLR, 2023).

2. Datasets used for the validation of EnMAP products

The primary data sources involved in the EnMAP validation are the EnMAP acquisition products and the reference or in-situ data. Care has been taken to ensure global and parameter-wise well-balanced validation sites (encompassing different targets) and in-situ data to make the validation representative.

2.1. EnMAP acquisitions and products

Since all validation tasks should be performed from a user's perspective, radiometric, spectral, reflectivity, geometric, and general uniformity of the three official EnMAP data products (L1B, L1C, and L2A) are validated based on the official standard products freely accessible to the users and obtained via the official online portal (DLR, 2023). Prioritized validation acquisitions with a maximal off-nadir pointing of 15 were acquired closely with scheduled in-situ measurements at predefined sites to generate validation-suitable match-ups. During CP, a considerable coordination effort was made, and significant acquisition capacities were used for generating validation acquisitions. During OP, the match-ups were generated besides the regular user-driven acquisition schedules and with the support of the user community. The data products used in this study refer to various calibration and processor versions. With regard to the archived (≥ V01.05.02) and preprocessing (≥ V01.05.02) versions, the integrated EO data tiles are to be as consistent, up-to-date, and advanced as possible. Minor problems have all been fixed in these versions. The continuous improvement of data quality from the CP to the current OP is indicated, but cannot be fully presented in this context. The results, therefore, relate to the mentioned data product versions currently available to the user at the time of the study. The validation includes 106 Level 1B, 187 Level 1C and 125 Level 2A products.

2.2. Reference measurements

Fig. 1 indicates the validation scenarios based on reference data in green. Two main types of references are used for the presented validation framework: Surface reflectance measurements and orthoimage references. The space-and-time-collocated in-situ BOA absolute reflectance measurements covering the entire EnMAP wavelength range in an adequate spectral resolution are difficult to access and elaborate. Two sources for reflectance measurements were used: Science-orientated measurement campaigns and continuous station measurements from the networks RadCalNet and HYPERNETS. The extensive support by validation field activities and stations forms the basis of the respective validation of L1B and L2A products, and the availability represents a tremendous and valuable community success.

2.2.1. Reflectance measurements on land

Table S2 in the Supplementary Material provides an overview of all land validation sites, including their location, land cover, number of EnMAP–in-situ match-ups. The in-situ land references comprise data from the RadCalNet stations Gobabeb (GONA) (Bouvet et al., 2019; Bialek et al., 2016), La Crau (LCFR) (Bouvet et al., 2019) and Baotou Sand (BSCN), as well as the HYPERNETS station Gobabeb (GHNA) (De Vis et al., 2023). The RadCalNet site Railroad Valley (RVUS) was excluded due to pronounced temporal variability in surface moisture and evaporitic crust formation (Czapla-Myers et al., 2008; Miura et al., 2021; Tahersima et al., 2025), which enhance bidirectional reflectance distribution function (BRDF) effects and cause irregular reflectance changes, particularly in the SWIR domain, thereby potentially biasing the overall validation statistics. The land cover at Gobabeb, Namibia, consists of gravel plains with occasional grass growth, while the land cover at BSCN, China, is desert sand, and at LCFR, France, thin pebbly soil with seasonally sparse vegetation. Measurements at GONA and LCFR cover the full EnMAP spectral range (400–2400 nm), measurements at GHNA cover only the spectral range 380–1680 nm, and those at BSCN are limited to 380–1080 nm.

In addition, coordinated field campaigns were performed synchronously to EnMAP acquisitions following the EnMAP Field Guide – In-Situ Measurements for Validation Purposes (Brell et al., 2023). These field campaigns comprise the arid desert sites Amiaz Plain and Makhtesh Ramon in Israel (Heller Pearlshtien and Ben-Dor, 2022), Pinnacles in Australia (Ong et al., 2017) and Black Rock Playa site in Nevada (Thompson et al., 2024). Furthermore, the agricultural sites Barrax and Camarena in Spain and Munich North Isar in Southern Germany. Finally, the Nansen Ice Shelf site in Antarctica (Di Mauro et al., 2024), the mixed grassland and oaktree site Majadas del Tietar in Spain and the artificial TXL Airfield site, which is part of the runway of Berlin Tegel airport, have been used.

Together, these land sites cover agricultural areas, bare soils, snow, and artificial surfaces, thus representing a broad range of reflectance levels. Figs. S1 and S2 in the supplementary show representative in-situ and EnMAP spectra for each site. For the L2A surface reflectance validations, the complete set of sites was considered. To minimize atmospheric uncertainties during the propagation of in-situ reflectance measurements to the top-of-atmosphere level, the L_{TOA} validation was restricted to the arid sites Pinnacles, Amiaz Plain, GONA, GHNA, Makhtesh Ramon, and Black Rock Playa Zero.

2.2.2. Reflectance measurements over water

For water validation, space-and-time-collocated match-ups were generated using a 3 by 3 pixels box and a time window of ±40 min from the overpass. The in-situ measurements for the water validation comprise the automated hyperspectral radiometry station measurements from the Lucinda Jetty Coastal Observatory (LJCO) in Australia (Schroeder et al., 2022; Brando et al., 2010) and the REmote Sensing for Trasimeno lake Observatory (RESTO) (Bresciani et al., 2020; Giardino et al., 2020) in Italy. Additional measurements were obtained from HYPERNETS network stations Acqua Alta Oceanographic Tower (AAOT) (Bracaglia et al., 2019) and Lampedusa (Ruddick et al., 2022) in Italy, and Oostende in Belgium (Vansteenwegen et al., 2019). These datasets were further complemented by science-oriented field campaigns conducted over Lake Constance (Bracher et al., 2021), the Río de la Plata in Argentina (Dogliotti et al., 2024), and the Magest site in France (Doxaran et al., 2024). Table S3 summarizes the water validation sites, their locations, and the number of match-ups. Most of these sites were also included in the previous validation work by (Soppa et al., 2024), but the dataset has been further expanded here.

2.2.3. Data filtering and quality control

Despite the high quality of the RadCalNet data, an internal quality and plausibility check of all EnMAP-aligned in-situ measurements was conducted, to ensure their suitability for validation. During the filtering three match-ups had to be rejected for the validation: The measurement at GONA on 2023/12/05 showed extremely low field reflectance, which is most probably due to an instrument failure. The measurements on 2022/09/17 and 2023/11/23 at LCRF showed reduced field reflectance in the SWIR spectrum, which is probably connected to increased soil moisture. The resulting 50 match-ups, that were used for BOA reflectance and L_{TOA} validation over land are listed in Table S4.

For water reflectance validation the match-ups were quality-controlled following the recommendations from the OLCI match-up protocol (EUMETSAT, 2022). The number of match-ups remained unchanged, as none were rejected during quality control. The 63 match-ups that were used for the water reflectance validation are listed in Table S5.

2.2.4. Orthoimage references

High-spatial-resolution orthoimage reference data, for which a higher spatial accuracy can be expected, was used for the absolute geometric validation. The used reference images consist of various publicly available sources (Google, 2023; Bing, 2023). Since the EnMAP geometric calibration is optimized scene-by-scene to a Sentinel-2 reference in the preprocessing as soon as matching is possible, care was taken in the geometric validation to use independent adequate reference data with a higher spatial resolution and accuracy. Plausibility checks and cross-checks between publicly available sources with Sentinel-2 ESA Global Reference Image (GRI) (ESA, 2023) were performed to ensure the higher spatial accuracy of the references used.

3. EnMAP validation tasks: Scientific background and methodology

All important validation tasks performed within the independent EnMAP validation are presented in the following sections in an EnMAP product-specific manner. The validation tasks can be categorized into radiometric, spectral, and spatial tasks congruent to Fig. 1. In principle, a methodological attempt was made to separate the radiometric, spectral, and spatial influences on the data quality from each other so that the respective effects on the data quality can be quantified separately.

3.1. Validation metrics

For characterizing the differences between the EnMAP L_{TOA} and BOA reflectance and the corresponding reference measurements, several validation metrics were applied, namely precision, accuracy and uncertainty. Accuracy is defined as the mean residual between the EnMAP-derived quantity and the corresponding reference measurement and therefore represents the systematic deviation (bias). Precision is defined as the standard deviation of the residuals and describes the dispersion of the differences around their mean, serving as an indicator of random effects. Uncertainty is defined as the root mean square error (RMSE) of the residuals and combines both systematic and random contributions. Residuals are computed depending on the product level: for radiance products as relative differences in percent with respect to the reference values, and for reflectance and water-leaving reflectance products as absolute differences.

3.2. L1B - product validation

The quality of the L1B-TOA radiance products is directly related to the overall sensor performance, as it is close to the sensor's raw measurement (L0) and independent of further processing steps. All derived subsequent products are based on this L1B product. Therefore, thorough radiometric, spectral, and spatial validations are performed, allowing the user to assess the quality of the general measurement and the subsequently derived products.

Regarding the radiometric quality of the L1B data products, the investigated radiometric parameters are the radiometric accuracy, signal-to-noise ratio (SNR), and spatially coherent artifacts (striping, bad and dead pixels). Since spectral information is crucial for an imaging spectrometer, its spectral characterization and uniformity are mandatory for its data's successful analysis and valorization. Therefore, EnMAP's spectral parameters and spectral response function are validated and monitored. The spatial parameter keystone is validated based on the L1B product in sensor geometry.

3.2.1. In-situ TOA radiance validation

The absolute TOA radiometric accuracy obtained after L0 processing is the most critical parameter in the validation of EnMAP L1B products since all other products are based on the quality achieved there. The L_{TOA} measured by the EnMAP satellite is validated by an EnMAP adopted reflectance-based approach (Fig. 3) (Thome et al., 2004; Green et al., 2003; Slater et al., 1996; Slater et al., 1987). Based on space-and-time-collocated ground-based BOA in-situ spectra, ideally simultaneously measured to an EnMAP acquisition, reference L_{TOA} spectra are calculated by atmospheric propagation using a combined radiative transfer (MODTRAN5 (Berk et al., 2006) LUT) and instrument and observation geometry model.

To perform the conversion from in-situ BOA reflectance to L_{TOA}, the Aerosol Optical Thickness (AOT) and Column Water Vapor (CWV) were required as atmospheric input parameters. The AOT values were available for all in-situ measurement sites, either provided by RadCalNet and HYPERNETS, or obtained from simultaneous aerosol measurements conducted during field campaigns at Pinnacles, Amiaz Plain, Makhtesh Ramon, and Black Rock Playa Zero. The CWV values are derived from the EnMAP L1B metadata, which provides scene-specific atmospheric water vapor content. The spatially corresponding EnMAP L_{TOA} measurement (pixel) is directly derived from the L1B products after a spatial optimization of the geolayer (based on a high spatial resolution georeference) and a neighborhood homogeneity check. Therefore, spatial resampling and spectral averaging do not take place. The propagated

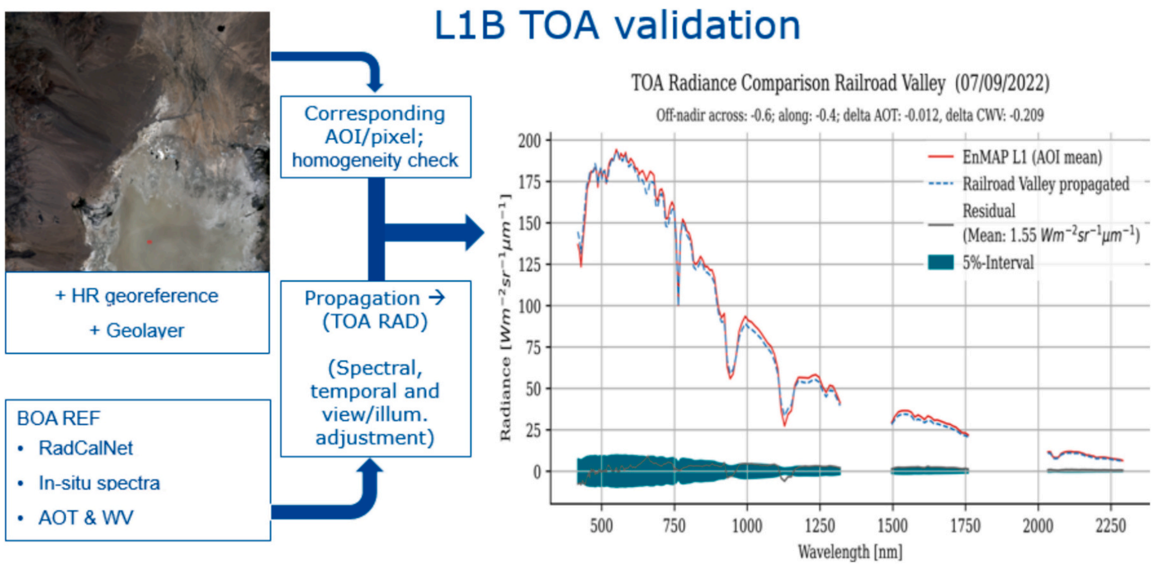

Fig. 3. Reflectance-based L1B TOA validation approach.

L_{TOA} spectra are then compared and statistically analyzed with the corresponding L_{TOA} measured by EnMAP.

The uncertainty, accuracy and precision are calculated for the measurements and analyzed regarding the mission requirements dependent on wavelength and radiance level. Based on the aggregated statistical analysis, systematic and random errors can be assessed and, in consequence, the validity and quality of the radiometric calibration.

3.2.2. Signal-to-noise ratio (SNR)

The achieved signal-to-noise ratio (SNR) is a key parameter for the accuracy and reliability of hyperspectral data analysis and interpretation. Therefore, the SNR was estimated for the VNIR and SWIR sensors based on 163 regular Earth acquisitions. The achieved SNR depends on several factors, including detector characteristics, optical system efficiency, illumination conditions, integration time, and dark current. Various methods exist to derive the effective SNR from hyperspectral data (Gao et al., 2013; Thompson et al., 2024). For EnMAP, instrument-based SNR estimates are derived from linearity calibration measurements and are regularly reported in the Mission Quarterly Reports (DLR, 2024).

These estimates are complementary to SNR values derived from actual Earth observations where the SNR was calculated for each scene and spectral band. For this purpose, homogeneous regions with low natural variability were automatically selected and subdivided into segments of 16 pixels. These segments were analyzed using the Discrete Cosine Transform (DCT) technique (Mustafa et al., 2019; Oktem and Ponomarenko, 2007; Pogrebnyak and Lukin, 2012).The segments were grouped into radiance bins, and the most representative bin, defined as the bin containing the largest number of samples, was selected for further analysis. The highest-frequency DCT coefficient was interpreted as a proxy for noise, while low-frequency components were assumed to represent scene-related variability. The SNR was then calculated as:

$$SNR = \frac{mean(L_{TOA})}{\sqrt{variance\ (noise)}}$$

The observed SNR can be described as a combination of signal-dependent photon shot noise and an additive, signal-independent noise component. Knowing the latter component allows the SNR to be transformed to any given radiance level. Therefore, the additive noise component was derived from the observed SNR and the corresponding L_{TOA}. For this purpose, radiance was converted into electrons using a wavelength-dependent multiplication coefficient c, taken from the latest radiometric module of the EnMAP end-to-end simulator EeteS (Segl et al., 2012):

$$additive\ noise\ [e] = \frac{\left(L_{TOA}{}^2 c^2 - SNR^2 L_{TOA}\ c\right)}{SNR^2}$$

For the VNIR bands, two distinct clusters of the additive noise component were observed, corresponding to high-gain (low radiance) and low-gain (high radiance) modes (see Fig. 4a). The threshold separating high-gain and low-gain modes was taken from instrument characterization (Fig. 4b) and separates both clusters almost perfectly.

To enable direct comparison with mission requirements defined for a 30% reflective target, the scene-based SNR estimates were converted to a reference-equivalent SNR (SNR_{ref}). Furthermore, it is evident that the method used to estimate the SNR exhibits a certain degree of variability, making a large sample size necessary. Therefore, the median value of the additive noise for the measurements was used for the further estimation of SNR_{ref}:

$$SNR_{ref} = \frac{L_{TOA\,ref}{}^{*}c}{\sqrt{additive\ noise + L_{TOA\,ref}{}^{*}c}}$$

Here, L_{TOA}ref. corresponds to the radiance of a 30% reflective target, a solar zenith angle of 30°, columnar water vapor of 2 cm and a visibility of 40 km. Only observations with consistent gain conditions were considered, i.e., low-gain measurements were used when L_{TOA}ref. fell within the low-gain regime, and high-gain measurements were used accordingly.

Additionally SNR_{ref} was normalized to a spectral sampling interval (SSI) of 10 nm by scaling the radiance-to-electron conversion coefficient c to enable a direct comparison with mission requirements:

$$SNR_{ref} = \frac{L_{TOA\,ref}{}^{*}c^{*}\frac{10}{SSI}}{\sqrt{additive\ noise + L_{TOA\,ref}{}^{*}c^{*}\frac{10}{SSI}}}$$

where the SSI was derived as the difference between the center wavelengths of two consecutive spectral channels.

3.2.3. Spatially-coherent radiometric miscalibration (striping artifacts)

Hyperspectral applications, which often rely on spectral derivatives, are sensitive to spatially coherent radiometric miscalibrations, which result in striping patterns. Even though no explicit mission requirements have been defined for this quality parameter, spatially coherent radiometric calibration accuracy is an essential quality parameter for the

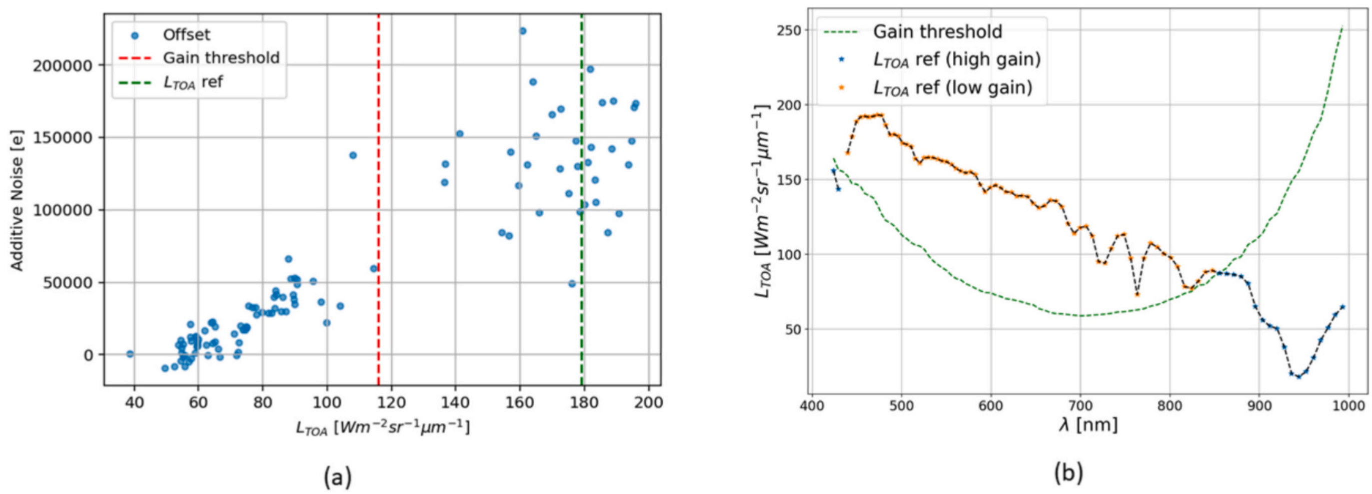

Fig. 4. Additive noise vs. L_{TOA} at 496 nm with gain threshold (red dashed) and reference L_{TOA} (green dashed) (a). The gain threshold and reference L_{TOA} for all VNIR channels are shown in (b). (For interpretation of the references to colour in this figure legend, the reader is referred to the web version of this article.)

users. Thus, an image-based detection and quantification of spatially coherent artifacts, which could cause striping patterns inside the L1B and thus also in the L1C and L2A products, is performed. The developed algorithm calculates across-track gradients and normalizes them by a local trend analysis. Destriping is achieved by estimating and removing column-wise radiometric biases after local trend normalization. For each spectral band, across-track gradients are computed, smoothed to capture the natural surface trend, and the residual mean offset per detector column is subtracted from the image. Band- and column-wise gain and offset deviations, as well as the mean radiometric miscalibration in percent, are then estimated based on the destriped and original data. With this approach, high-frequency and low-frequency band−/column-wise radiometric miscalibration can be detected. In addition, conclusions can be drawn about newly emerged bad and dead pixels.

3.2.4. Smile and full width at half maximum (FWHM)

Several methods have been proposed that utilize atmospheric absorption features for the spectral characterization of imaging spectrometers (Green, 1998; Neville et al., 2003; Green et al., 2003; Guanter et al., 2006). The across-track instrument spectral response variation in the wavelength center position (smile) and FWHM of a Gaussian spectral response function are characterized by modeling atmospheric absorption features in the L1B product. In particular, the oxygen A and methane absorption bands at 760 nm, and 2300 nm, respectively, are used to assess the spectral performance of the VNIR and SWIR spectrometers separately. Shifts from nominal center wavelengths and FWHM have been calculated separately for each across-track position for seven scenes. The method (Guanter et al., 2009; Guanter et al., 2006) estimates the center wavelength shift and FWHM variation across-track, leading to the smoothest surface reflectance spectrum after applying the atmospheric correction. The estimated across-track variation in the center wavelength allows the characterization of a potential spectral smile. The spectral characterization is assessed regularly using the OBCA as well as using atmospheric features and is documented in the Mission Quarterly Reports (DLR, 2024). The EnMAP mission requirement regarding the across-track uniformity of spectral channel positions is <20% linear displacement of a detector element.

3.2.5. Keystone (spatial across-track distortion)

The geometric counterpart to the smile is the band-to-band across-track spatial misregistration (keystone) caused by non-uniformity projection to the sensor array (Mouroulis et al., 2000). This pixel's spatial position variation with wavelength is one of the main parameters defining the data's general spatial consistency and must be validated in sensor geometry (L1B). The developed algorithm quantifies across-track spatial misregistration using a phase-correlation method in the Fourier domain between consecutive spectral bands. The algorithm computes sub-pixel shifts over areas with no spectral but spatial across-track gradients. The shifts are smoothed with a Gaussian filter and accumulated along the spectral dimension to obtain the cumulative band-wise displacement in pixels. The EnMAP mission requirement is congruent to the spectral across-track uniformity and < 20% linear displacement of a detector element.

3.3. L1C - product validation

All parameters related to the quality of the L1C product are closely linked to the geometric and pointing performance. Regarding the spatial quality of the L1C data products, the investigated spatial parameters are VNIR-to-SWIR co-registration and the absolute spatial georectification accuracy.

3.3.1. VNIR-to-SWIR spatial co-registration

To achieve consistent spectral information over the VNIR-SWIR wavelength domain, the VNIR-to-SWIR spatial co-registration is a critical quality parameter, especially for spatially heterogeneous surfaces. Since both sensors have slightly different Line-Of-Sights and are georeferenced separately, there is an intrinsic co-registration error due to the detector alignment residuals. Thus, the geometric calibration is done for both sensors separately to minimize the co-registration error. Spatially variable shifts between the spectrally close-by VNIR band 95 (∼968.6 nm) and the SWIR band 96 (∼972.3 nm), which can be expected to show very similar spectral content, were derived based on the Automated and Robust Open-Source Image Co-Registration Software (AROSICS). AROSICS is a Python framework for automated, sub-pixel accurate co-registration of remote sensing imagery based on phase correlation and robust outlier filtering (Scheffler et al., 2017; Scheffler, 2023). Spatially congruent patches regularly sampled from both bands are compared based on phase-correlation in the Fourier space. The determined tie points are then filtered by a three-step outlier detection approach featuring a reliability measure developed by the authors as well as power spectrum thresholding, RANSAC (Fischler and Bolles, 1981), and SSIM (Wang et al., 2004) techniques. Statistical measures per tile and an aggregation that includes several tiles are calculated. Investigated scenes should ideally cover definable edges and structures in the spatial scale of EnMAP and should be free of clouds. The mission requires a VNIR-to-SWIR spatial co-registration < 30% of a pixel. This mission requirement can be validated since the method can detect sub-pixel shifts with high accuracy.

3.3.2. Absolute spatial accuracy

For multitemporal, cross-satellite, or geoinformation comparisons and analyses, the absolute geometric accuracy of EnMAP is mandatory. Several factors, e.g., pointing accuracy and stability, micro-vibrations, Earth rotation, terrain, and the elevation model's quality, influence the achieved geometric EnMAP accuracy. The absolute spatial accuracy is determined by comparison with cloud-free orthorectified reference images of higher spatial resolution and accuracy, which map time-invariant contrasting surface patterns ideally homogeneously distributed over the whole scene. The used reference images (section 2.2.3) have been cross-checked with various sources and thus can be seen as geometrically highly reliable. Spatially variable shifts between the EnMAP L1C product and a reference are derived based on the AROSICS algorithm (Scheffler et al., 2017). The algorithm resamples the reference imagery to the EnMAP spatial resolution and filters the derived GCPs (see Section 1.4). Standard statistical shift measures (mean, standard deviation, RMSE) are derived separately for x and y and combined shifts. The single tile-based measures are then aggregated statistically for several tiles to get a stable misregistration statistic. If a reference optimization during the EnMAP preprocessing was possible, the mission requirement is < 1 GSD. If a reference optimization was impossible due to, e.g., clouds, snow, water, or lack of matching structure, the mission requirement is < 100 m

3.4. L2A - product validation

The quality of the L2A product is of central importance for most users and applications since it defines the quality of the measured surface reflectance. Since it is derived from the preliminary products by applying an atmospheric correction technique, the quality of the L2A products integrates all previous radiometric, geometric, and spectral quality characteristics.

3.4.1. In-situ BOA reflectance validation (land)

The mission requirements of surface reflectance (ρ) for EnMAP have been defined with regard to (Vermote and Kotchenova, 2008) based on uncertainties represented by the RMSE for different reflectance levels outside strong atmospheric absorption on flat and close-to Lambertian surfaces: < 0.01 for $\rho < 0.1$ and < 0.02 for $0.1 \leq \rho < 0.3$ and < 0.05 for $0.3 \leq \rho \leq 0.6$. Therefore, congruent to Section 3.2.1, RMSE, mean residual and standard deviation around mean measured values are calculated for the measurements and analyzed against the mission requirements wavelength and level dependent to assess systematic and random errors and thus the achieved quality of the available surface reflectance.

3.4.2. In-situ normalized water-leaving reflectance validation (water)

For the L2A Normalized Water-Leaving Reflectance validation, the in-situ measurements were provided as water-leaving reflectance (AAOT, Oostende, Lampedusa) and Remote Sensing Reflectance (sr-1). Remote Sensing Reflectance measurements were transformed to Normalized Water-Leaving Reflectance by multiplying by π. The EnMAP spectrum represents the median of a 3×3 pixel window after the outliers were removed. Congruent to Sections 3.2.1 and 3.4.1, uncertainty (RMSE), accuracy (mean residual), and precision (standard deviation around mean measured values) are aggregated for the residuals and plotted against the mission requirements wavelength and level dependent. The mission requirement is based on uncertainty (RMSE) outside strong atmospheric absorption regions, and for AOT at 550 nm < 0.4 is: < 0.04 for $400\,\text{nm} < \lambda \leq 450\,\text{nm}$; < 0.02 for $450\,\text{nm} < \lambda \leq 650\,\text{nm}$; < 0.01 for $650\,\text{nm} < \lambda \leq 800\,\text{nm}$. For AOT at 550 nm > 0.4, the corresponding requirement increases by 0.01.

4. Results of the EnMAP validation

Within the following, the independent validation results are presented for the 3 different processing levels.

4.1. L1B - product validation

4.1.1. In-situ TOA radiance validation

Based on the plotted wavelength-dependent L_{TOA} uncertainties (Fig. 5), it is identified that uncertainties and accuracies are slightly outside the mission requirements for the 420–550 nm wavelength domain of the VNIR sensor. EnMAP TOA measurements are systematically below the propagated in-situ measurements for many match-ups in this area, which could have two overlapping reasons. One is the higher radiometric uncertainty of the in-situ instrument due to the generally lower radiance level of artificial lighting used in the in-situ instrument calibration procedure (Helmlinger et al., 2016) compared to the EnMAP sun calibration. The other is AOT level dependent uncertainties (Carmon et al., 2020) introduced in the TOA propagation procedure. The values are also outside the requirements for $>$2200 nm in the SWIR, which could be addressed to higher uncertainties in the in-situ measurements due to very low radiance levels combined with CWV influences in this wavelength domain. Between 550 nm and 2200 nm, the measurements are inside the mission requirements. A systematic tendency to higher EnMAP radiances is identified for the SWIR sensor response (1000–2300 nm), and uncertainties are at the edge of the mission requirements.

A similar pattern is seen for the radiance level-dependent statistic (Fig. 6). The accuracy is inside the 5% requirement for most of the radiance levels. However, uncertainties lie at the upper edge of the requirements, mainly driven by the precisions for the radiance levels up to 150 [W/m^2/sr/μm], where a sufficient sample frequency is available. For the higher radiance levels $>$150 [W/m^2/sr/μm], all three statistical measures are reduced apart from some bins driven by higher AOT-induced uncertainties for snow match-ups in the shorter wavelengths. However, the number of samples is relatively small for these levels.

4.1.2. Signal-to-noise ratio (SNR)

Fig. 7 (a) and (b) show the reference-equivalent SNR (SNR_{ref}, red) and the SNR_{ref} normalized to an SSI of 10 nm (black) for the VNIR and SWIR channels, respectively. Both were calculated as described in Section 3.2.2 and correspond to the radiance level of a 30% surface reflectance target, enabling direct comparison with the defined mission SNR requirements.

At 496 nm (Fig. 7a), SNR_{ref} reaches 369:1, while the normalized SNR_{ref} reaches 597:1. Hence, the VNIR SNR requirement ($>$ 500:1, Table 3) is fulfilled. At 2200 nm, SNR_{ref} reaches 255:1 and the normalized SNR_{ref} reaches 279:1, thereby also fulfilling the SWIR SNR requirement ($>$ 150:1, Table 3). Overall, the results demonstrate that the achieved SNR meets and exceeds mission requirements, indicating a robust basis for a wide range of applications.

4.1.3. Spatially-coherent radiometric miscalibration (striping artifacts)

96 different L1B tiles were analyzed regarding across-track anomalies. Initial inherent and randomly distributed high-frequency across-track anomalies are suppressed efficiently to a shallow level ($<$1%) for all tiles with a preprocessor version greater than V01.02.00. However, inherent low-frequency across-track artifacts with a shallow radiance level are still detected. They can be interpreted as band/column inherent undulations that affect more than a single column and are not as easy to detect visually as well as quantitatively compared to the high-frequency features. For both VNIR (Fig. 8 (a)) and SWIR (Fig. 8 (b)), the mean radiometric miscalibration in percent indicates a relatively stable across-track pattern for all bands in the VNIR and SWIR. It also shows that the gain match is small, and the pattern is mainly additive/offset-driven.

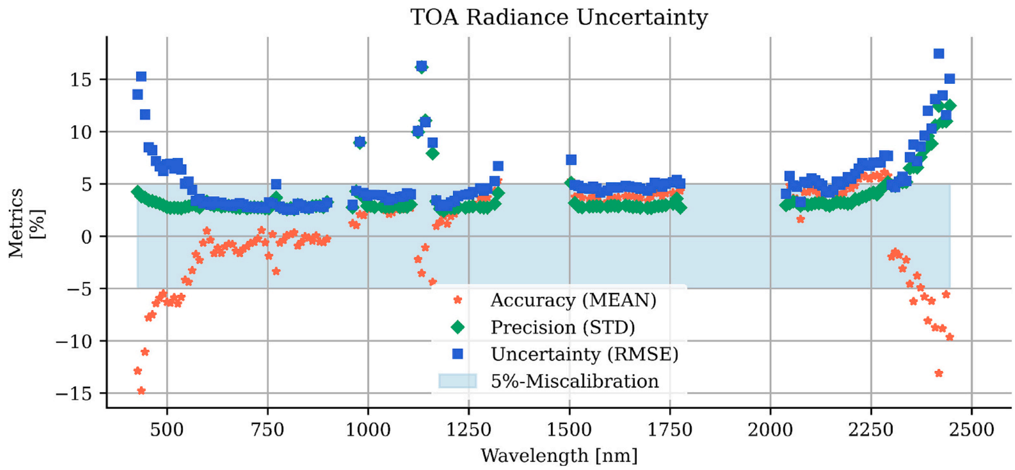

Fig. 5. Wavelength-dependent TOA radiance uncertainties, accuracies and precisions based on 33 match-ups.

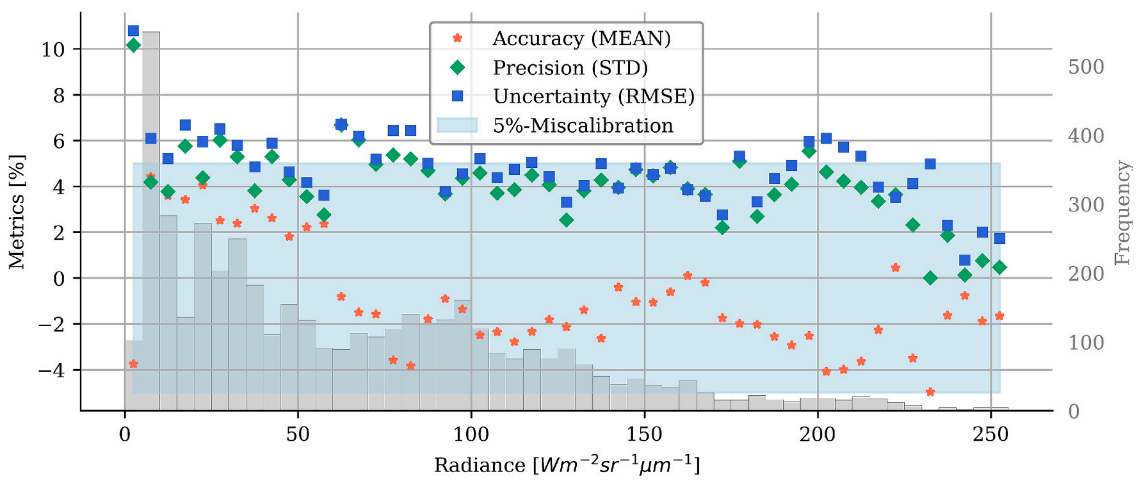

Fig. 6. Radiance level-dependent TOA radiance uncertainties, accuracies, and precisions based on 33 match-ups.

The complete statistical analysis indicates that the quantitative characteristic has little variability. A visual inspection of various homogeneous scenes (over different targets) confirms the low-frequency artifacts distinct from their direct neighbors. The mean delta offset plot for the VNIR (Fig. 8 (a)) also confirms (Storch et al., 2023) a slight inherent fringing (etaloning) effect from band ∼75 onwards. The mean radiometric miscalibration in percent determines that the spatially coherent across-track artifacts are rather minor and inside the radiometric mission requirements of <5%. Natural surface trends showing through due to image-based derivation cannot be excluded. However, due to the averaging of the derived across-track anomalies over 96 different tiles, the potential influence of natural surface properties can be considered low.

4.1.4. *Smile and full width at half maximum (FWHM)*

A total of seven different tiles were analyzed for this independent validation task (Fig. 9). The scene-based estimates of across-track spectral position variations are relatively small for both 760 nm and 2300 nm concerning the instrument SSD. The across-track shapes of the spectral shift and FWHM curves are almost identical for all seven analyzed acquisitions, but the absolute values change from tile to tile by 0.1–0.2 nm. A fraction of this is likely associated with method-related biases, especially for the relatively narrow 761 nm feature. For the VNIR (761 nm feature), the SSD is ∼7.3 nm, and the across-track amplitude of estimated $\Delta\lambda$ is ∼0.3 nm, which corresponds to a linear displacement of a detector element of ∼4.1% and thus follows the mission requirement of $<$ 20%. The wavy $\Delta\lambda$ changes at the edges can be attributed to the fringing effects in this detector area. For the SWIR (2300 nm feature), the SSD is around 8.0 nm, and the across-track amplitude of estimated $\Delta\lambda$ is ∼1.0 nm, which corresponds to a linear displacement of a detector element of ∼12.5% and thus likewise fulfills the mission requirement. The VNIR SSD is smaller than the FWHM, resulting in a slightly smoother spectral signal than the achieved SSD delivers (Fig. 2); for the SWIR SSD, the opposite is the case. The across-track $\Delta FWHM$ is also very small for both features. The amplitude for VNIR (∼0.4 nm) and SWIR (∼0.8 nm) results in a respective displacement of a detector element of 6.5% and 10%.

4.1.5. *Keystone (spatial across-track distortion)*

The 36 different tiles were analyzed for this validation task separately for VNIR (Fig. 10 (a)) and SWIR (Fig. 10 (b)). The detected spatial across-track shift cumulated along bands amplitude results in 7.2% of a pixel for the VNIR detector (Fig. 10 (a)) and 8.1% of a pixel for the SWIR detector (Fig. 10 (b)). The across-track amplitude for the single bands is also negligibly small. Such small spatial non-uniformities detected amplitudes are at the algorithm's inherent detection limits. Still, the algorithm would detect significant shifts, and systematic trends regarding keystone would be unmasked by the averaging based on 36 tiles. Therefore, it can be concluded that both sensors are very well inside the mission requirements of $<$ 20% linear displacement of a detector element and that this small inherent keystone pattern can be neglected from an end-user point of view.

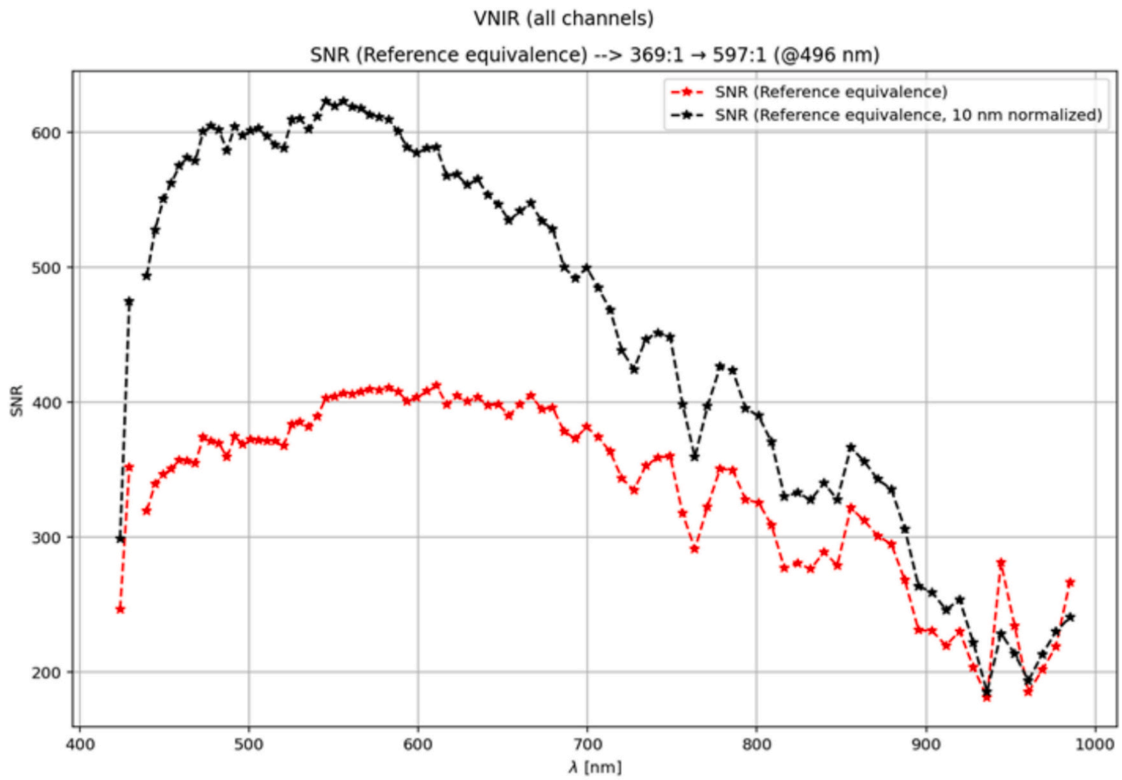

(a)

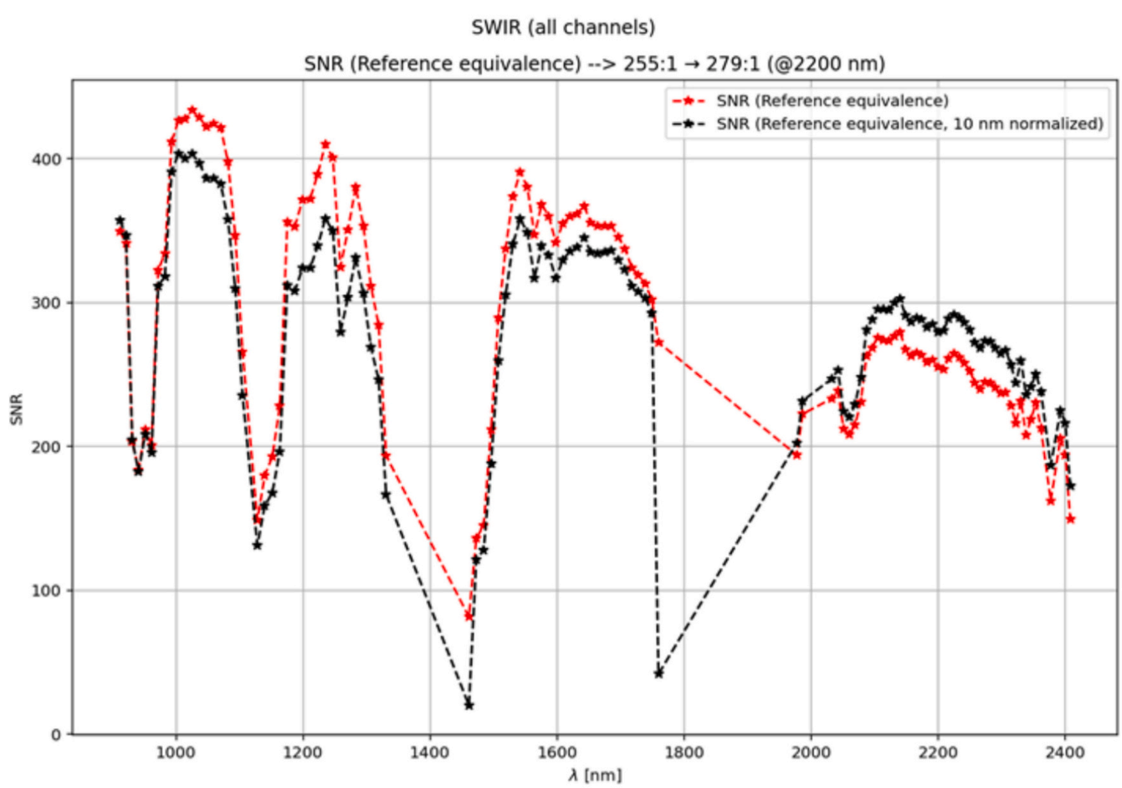

(b)

Fig. 7. (a) SNR estimation for VNIR based on 106 tiles; SNR (reference equivalent) 369:1 @ 496 nm; SNR (normalized reference equivalent) 597:1 @ 496 nm and (b) SNR estimation for SWIR based on 98 tiles; SNR (reference equivalent) 255:1 @ 2200 nm; SNR (normalized reference equivalent) 279:1 @ 496 nm.

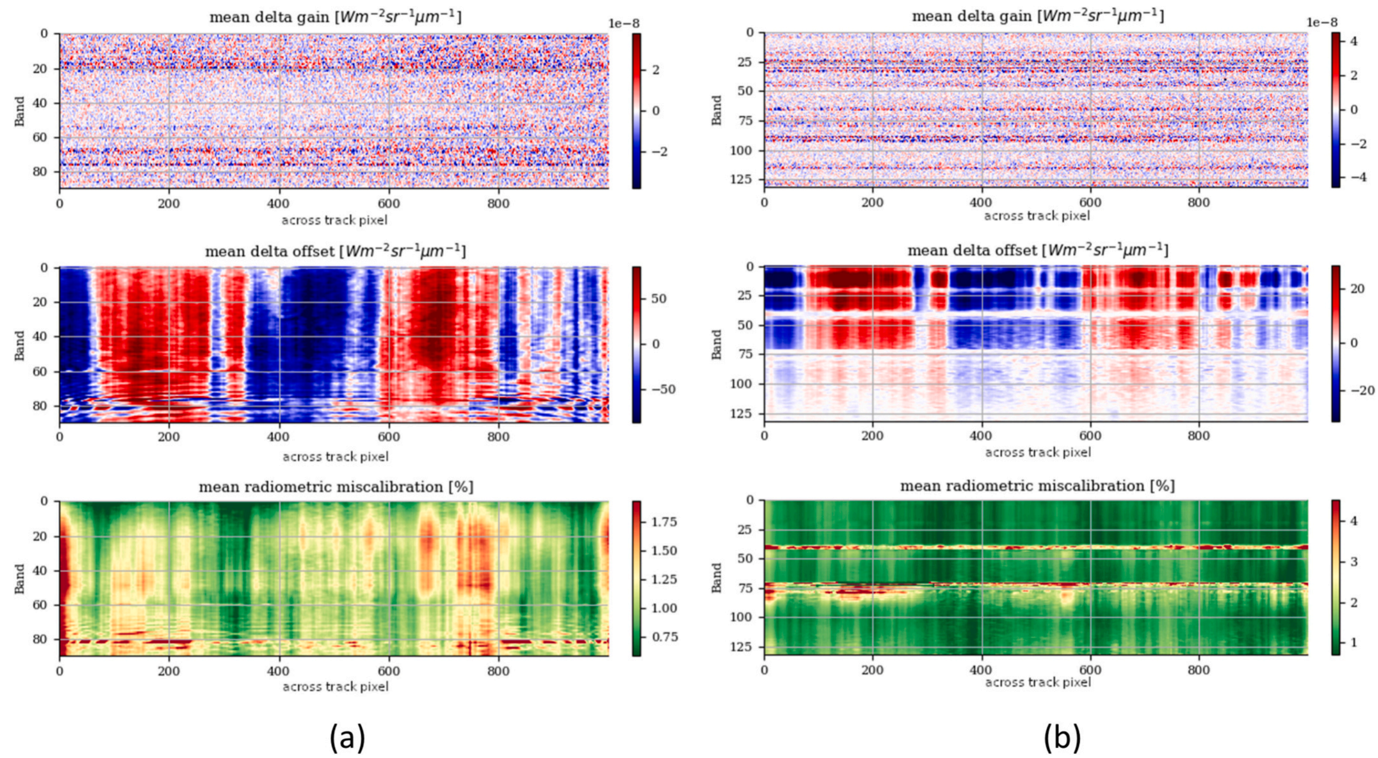

Fig. 8. Mean low-frequency across-track anomalies for (a) VNIR and (b) SWIR based on 96 tiles.

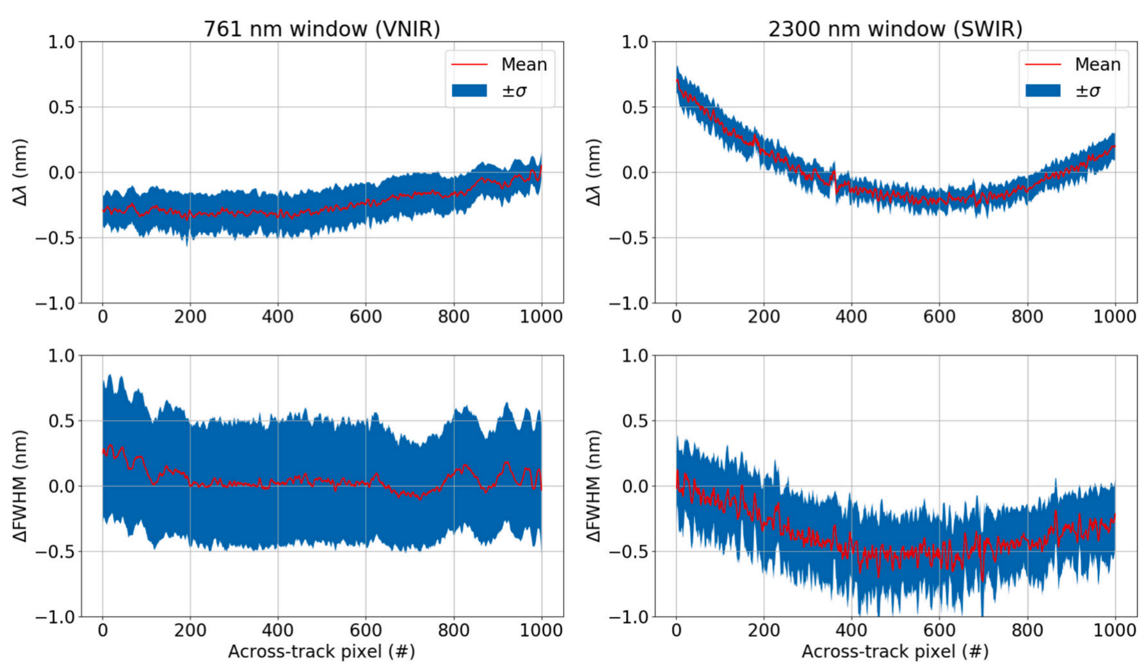

Fig. 9. Approximated relative smile and FWHM for 760 nm (VNIR) and 2300 nm (SWIR) based on seven tiles.

4.2. L1C - product validation

4.2.1. VNIR-to-SWIR spatial co-registration

For this validation task, a total of 110 suitable tiles were analyzed (flat as well as mountainous regions). An aggregated relative spatial accuracy statistic was generated processed with the current geometric calibration (Table 1). The RMSE in the x-direction (6.05 m) and y-direction (6.42 m) fulfill the requirements of the mission of $<$ 30% of a pixel. For acquisitions acquired before 03.11.2022, the official reprocessing of the L0 archive (archived version $\geq$ 01.03.00) fixed the geometric calibration issues before that date. Therefore, only products with an archived version $\geq$ 01.03.00 should be used to avoid VNIR-SWIR spatial inconsistencies.

4.2.2. Absolute spatial accuracy

A total of 187 different EnMAP file tiles were analyzed for this validation task. An aggregated absolute spatial accuracy statistic was generated based on these tiles (Table 2). The RMSE in the x-direction

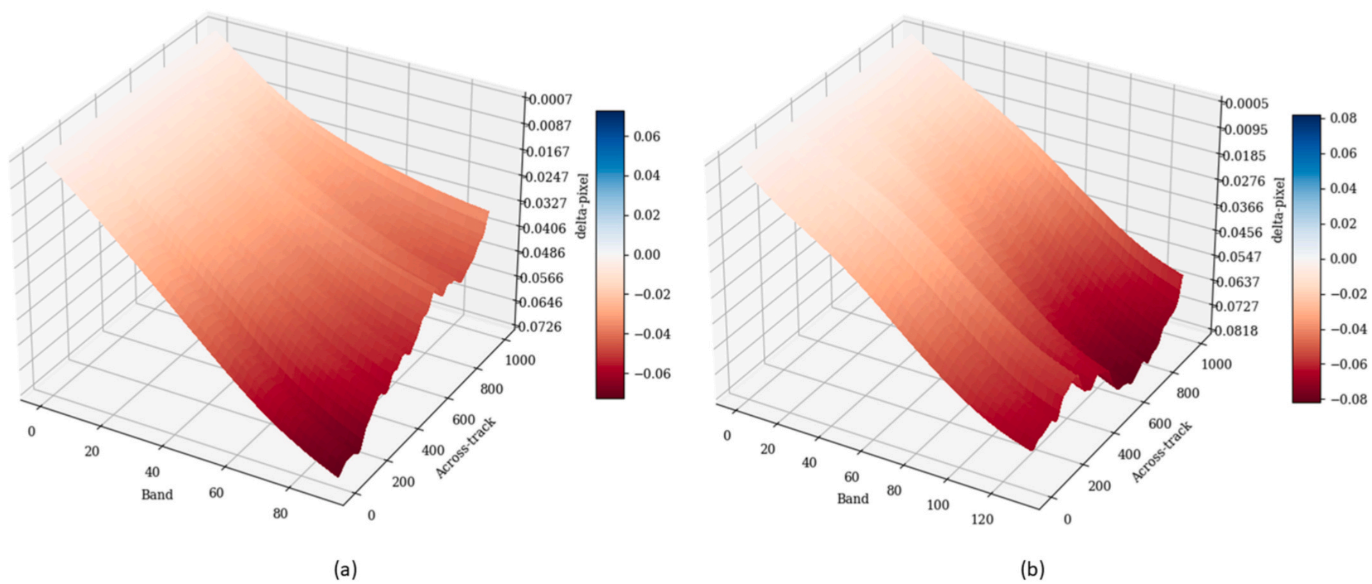

Fig. 10. VNIR (a) and SWIR (b) keystone; pixel-based across-track distortion cumulated along bands based on 36 tiles.

Table 1
Aggregated VNIR-to-SWIR spatial co-registration statistics based on 110 tiles.

Metric	Value [m]
MEAN XY	8.81
MEAN X	−5.2
MEAN Y	4.64
STD XY	1.41
STD X	2.1
STD Y	2.43
RMSE XY	8.94
RMSE X	6.05
RMSE Y	6.42

Table 2
Aggregated absolute spatial accuracy statistic based on 187 tiles.

Metric	Value [m]
MEAN XY	16.44
MEAN X	−0.83
MEAN Y	3.28
STD XY	5.51
STD X	5.7
STD Y	7.28
RMSE XY	17.56
RMSE X	10.46
RMSE Y	13.49

(10.46 m) and y-direction (13.49 m) are both inside the mission requirements of 30 m (1 GSD) for reference-optimized tiles. Tiles that were not optimized could not be validated due to the lack of reliable GCPs.

4.3. L2A - product validation

4.3.1. In-situ BOA reflectance validation (land)

Based on the plotted wavelength-dependent BOA reflectance statistic measures (Fig. 11), we see that the uncertainties, accuracies, and precisions are, in principle, < 3% for both the VNIR and the SWIR wavelengths range. The dispersion around the references (precision) increases significantly in the 400–500 nm wavelength domain. This can be due to the influences of aerosols and a lack of Dark Dense Vegetation (DDV) for 39 of the match-ups, which is associated with a fallback to a standard atmosphere (visibility of 23 km (de los Reyes et al., 2020)) in the L2A atmosphere correction. Only eleven in-situ measurements have sufficient DDV (at least 2% of all pixels (de los Reyes et al., 2020)) to approximate and incorporate correct AOT. The analyses also used tiles and match-ups without DDV and assumed standard atmosphere to generate stable validation statistics.

The mean residual (accuracy) indicates a slight underestimation of EnMAP in the shorter wavelength of the VNIR, which is also due to the lack of AOT compensation. When interpreting the results in this wavelength area, the higher inherent uncertainties must also be considered due to in-situ calibration limitations (Helmlinger et al., 2016). For the SWIR part, the EnMAP-derived reflectance is systematically higher than the in-situ reflectance values. This trend turns into the opposite beyond 2300 nm, where increased dispersion can be addressed to increased H_2O influences. Generally, slightly higher residual dispersions around the main atmospheric features (e.g., O_2 A ∼762 nm, H_2O, and CO_2) are visible. All indicated patterns are consistent with the individual L_{TOA} comparisons. Nevertheless, the wavelength-based statistical assessment indicates a high and stable EnMAP L2A product quality within the accepted mission requirements.

A corresponding pattern can be seen for the level-dependent BOA reflectance statistic (Fig. 12). Uncertainties for small reflectance levels (< 10%) are well within the mission requirements (< 1%). Small overshoots can be detected for reflectance levels of 10–15%. This can be explained by the dominance of the shorter wavelengths for these reflection levels and the lack of real inherent AOT compensation for most used tiles. Reflectance levels > 15% are strictly under the respective 2% and 5% requirements. Only levels > 80% have a higher dispersion. However, one can see from the frequency histogram in Fig. 12 that the statistics are only based on few measured values and are thus unreliable compared to the lower reflectance levels.

4.3.2. In-situ normalized water-leaving reflectance validation (water)

The water validation is based on 63 EnMAP tiles. 4 tiles from the commissioning phase are classified as low quality by the GS, but they were included here in the statistics as the RMSE was inside the requirements. Overall, EnMAP Normalized Water-Leaving Reflectance products underestimate the in-situ measurements. Higher uncertainties are observed at shorter wavelengths (< 500 nm) due to the stronger influence of the atmosphere by aerosol and molecular scattering. Nevertheless, the wavelength-dependent plot of uncertainty, precision, and accuracy in Fig. 13 indicates that all mission requirements are

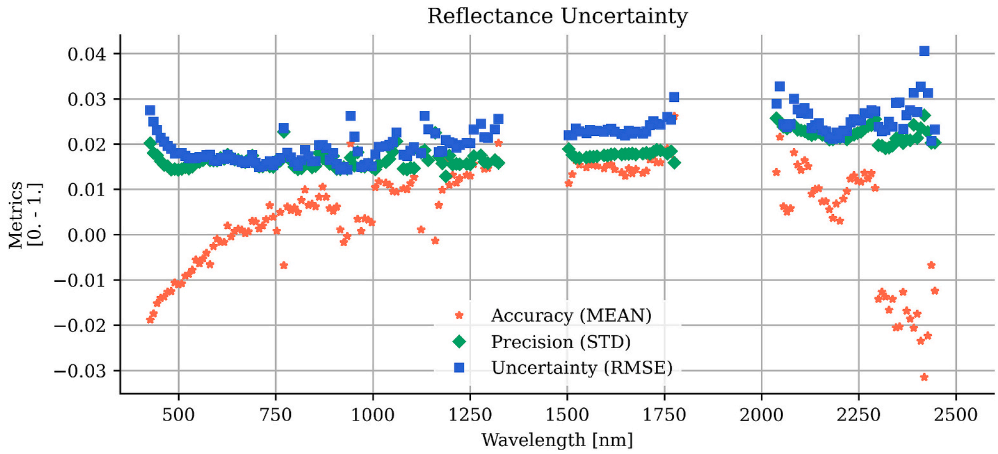

Fig. 11. Wavelength-dependent BOA reflectance uncertainties, accuracies, and precisions based on 50 match-ups.

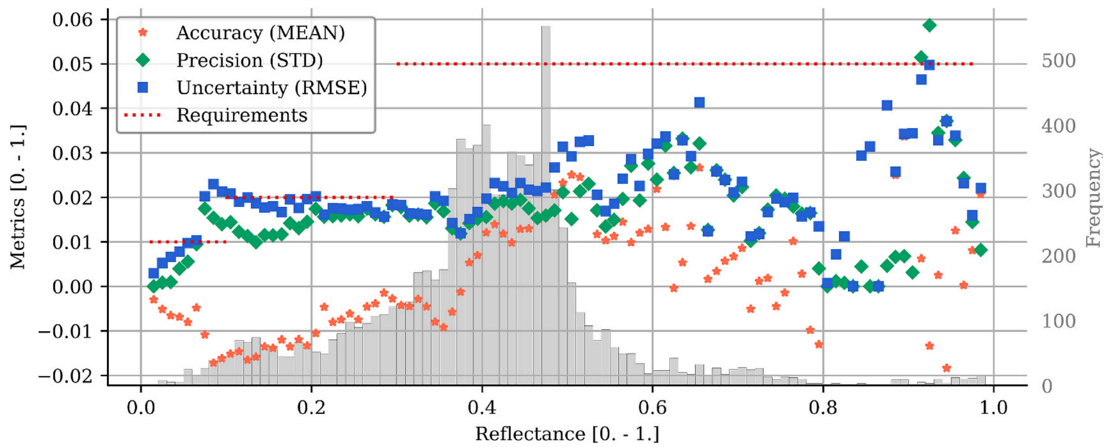

Fig. 12. Level-dependent BOA reflectance uncertainties, accuracies, and precisions based on 50 match-ups.

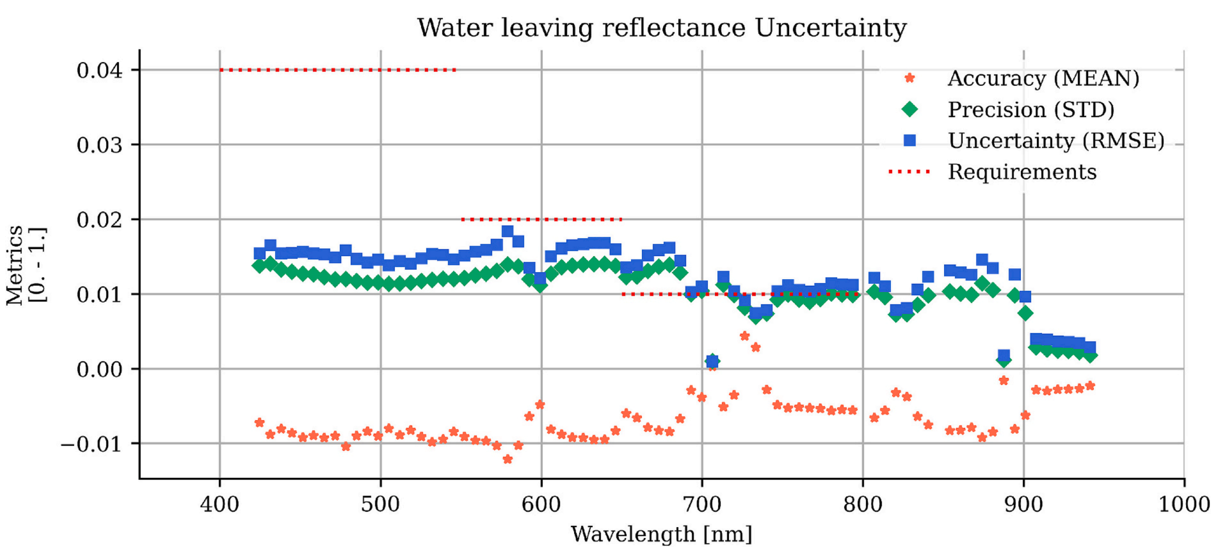

Fig. 13. Wavelength-dependent Normalized Water-Leaving Reflectance uncertainties, accuracies, and precisions based on 63 match-ups.

fulfilled without constraints.

Also, for the level dependent uncertainty (Fig. 14), it can be seen that the lower reflectance levels are below 1% uncertainty, and for the levels > 0.02, well below 2%. Only levels > 0.08 have a higher dispersion. However, such high normalized water-leaving reflectance values are less frequent in water surfaces, as confirmed by the frequency histogram in Fig. 14.

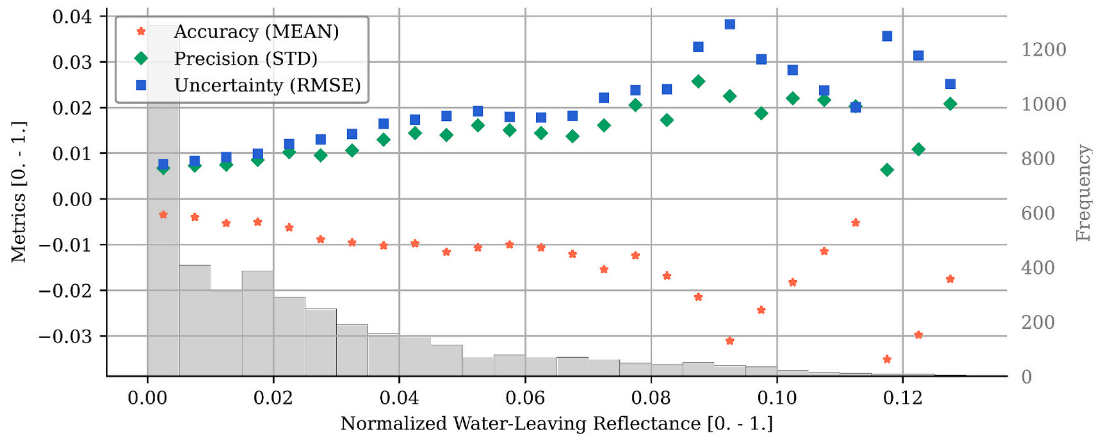

Fig. 14. Level-dependent Normalized Water-Leaving Reflectance uncertainties, accuracies, and precisions based on 63 match-ups.

5. Discussion and conclusion

5.1. Discussion of the results

The validation results confirm the high quality and reliability of the EnMAP products across all processing levels. For the Level-1B products, the validation of SNR, keystone, and spectral smile showed results that are well within the defined mission requirements. The validation of radiometric calibration also indicates that the requirements are generally met. However, shallow low-frequency across-track artifacts (striping) were observed in some scenes. These low-frequency across-track artifacts could potentially influence the user's thematic products and quantitative determination of bio-physical and bio-chemical parameters to a certain degree. Therefore, the aim is to investigate these effects in greater depth and, where possible, to eliminate them in the future.

The in-situ L_{TOA} validation confirms that EnMAP's radiometric performance is generally within the mission requirements, with slightly elevated uncertainties in the 420–550 nm and >2300 nm regions due to low radiance levels, calibration limitations, and AOT-dependent propagation effects. Across 550–2300 nm, EnMAP radiances show stable behavior with a minor systematic positive bias in the SWIR range and uncertainties near the upper edge of the mission thresholds. As the small overshoots can be caused by increased uncertainties in the in-situ measurements and the propagation of the in-situ reflectance to TOA level they are not considered to compromise the mission requirements. More accurate and specific findings must be obtained based on further scenarios during the ongoing operational phase. The indicated radiometric quality of the L1B products provides a solid basis for further derived products and applications.

The spatial validations, including VNIR-to-SWIR co-registration and absolute spatial accuracy, also yielded results that are well within the respective mission requirements, confirming the excellent geometric performance of the EnMAP sensor system.

Similar to the L_{TOA} validation, the BOA reflectance validation is generally within the mission requirements, with slightly increased uncertainties in the edge wavelength regions (420–550 nm and >2300 nm) and a tendency of EnMAP to produce slightly higher reflectance values in the SWIR range. The overall quality of the BOA reflectance products provided to users is therefore solid and sufficient for most scientific applications and for the generation of higher-level products. In addition, the Normalized Water-Leaving Reflectance validation confirms that the product quality fully meets the high demands of aquatic applications as reported in (Soppa et al., 2024), with uncertainties well below the specified limits across all relevant reflectance levels.

5.2. Uncertainty of the in-situ reference measurements

The in-situ reference measurements used for EnMAP validation are not free of error and should not be regarded as absolute “truth.” Their uncertainties vary depending on the measurement source and processing. The RadCalNet sites comply with QA4EO principles, ensuring SI traceability and site-to-site consistency, with BOA and TOA uncertainties typically below 5% outside strong atmospheric absorption features (Bouvet et al., 2019). HYPERNETS propagates random and systematic uncertainties through a Monte Carlo approach (De De Vis et al., 2024).

While full uncertainty traceability was planned, it could not be fully realized during the Commissioning and Operational Phases due to resource constraints. Errors were minimized according to the EnMAP Field Guide (Brell et al., 2023), and only reference data meeting mission uncertainty requirements were included.

Field campaign data, though valuable, lack standardized uncertainty traceability. Instrumental errors such as calibration drift, stray light, or temperature effects, and comparison errors due to spatial mismatch or heterogeneous surfaces, contribute additional uncertainty. Nevertheless, the large number and diversity of measurements are expected to compensate each other concerning systematic and random errors to a certain degree.

Standards for in-situ data acquisition for satellite validation over water sites, as defined in (IOCCG, 2019), were followed for all EnMAP match-up measurements in this study as well as in the first validation study of EnMAP L2A water reflectance data (Soppa et al., 2024). Intercomparison efforts quantifying differences between instruments, instrumental setups, and data processing have been carried out within the framework of the ESA and EUMETSAT FRM4SOC project and the HYPERNETS project, funded by the European Union's Horizon 2020 program, through various activities (FRM4SOC, 2020; Ruddick et al., 2025; Vabson et al., 2024). The results were incorporated into the HYPERNETS data processor enabling a good approximation of the uncertainty to these reference data (De De Vis et al., 2024).

To ensure independence, no data used for EnMAP calibration were employed for validation. All calibrations rely on on-board systems, with vicarious calibration limited to geometric adjustments. The reported EnMAP quality estimates therefore represent conservative lower bounds of the actual sensor performance, as part of the residual error originates from the reference data themselves.

5.3. Conclusion

A holistic characterization of the essential EnMAP product parameters has been realized based on EO acquisitions only and, where necessary, supported by adequate in-situ measurements. All key radiometric, spectral, geometric, and reflectance parameters characterizing the EnMAP product quality match the agreed mission requirements well and indicate an excellent product quality effectively available for the users in Table 3.

The general focus of the validated product parameters was on absolute quality, also based on in-situ measurements to determine the current status of data quality. Although the stability between two consecutive calibrations, preprocessing changes, and short outages were monitored during CP and OP, and a continuous and sustainable improvement in product quality was observed at the various levels, only the status of the current product quality fit the scope of this paper. With the increasing aging of the instrument and the onboard calibration devices (e.g., sun diffuser), the analyses will focus more on relative stability and comparability over time regarding particular sites and the relative categorization across missions in the future.

Quantifying and characterizing the EnMAP product's quality is a crucial part of guaranteeing transferability and thus enables improved interpretation of the information content application-wise. As the findings of the independent EnMAP product validation are continuously incorporated into improving the data quality, the validation efforts make a vital contribution to EnMAP data quality and support the general success of a hyperspectral EO mission. Overall, we can state that EnMAP mission represents an important step forward in the field of space imaging spectroscopy and can significantly contribute to develop higher level products and new applications in different domains.

CRediT authorship contribution statement

Maximilian Brell: Writing – review & editing, Writing – original draft, Visualization, Validation, Supervision, Software, Resources, Project administration, Methodology, Investigation, Funding acquisition, Formal analysis, Data curation, Conceptualization. **Philipp Reiners:** Writing – review & editing, Software, Methodology, Investigation. **Luis Guanter:** Writing – review & editing, Supervision, Software, Methodology. **Karl Segl:** Writing – review & editing, Supervision, Software, Methodology, Funding acquisition. **Sabine Chabrillat:** Supervision, Funding acquisition. **Daniel Scheffler:** Writing – review & editing, Software, Methodology. **Mariana A. Soppa:** Writing – review & editing, Supervision, Software, Methodology. **Niklas Bohn:** Writing – review & editing, Software. **Javier Gorrono:** Writing – review & editing, Software. **Alexander Kokhanovsky:** Writing – review & editing. **Astrid Bracher:** Writing – review & editing. **Martin Bachmann:** Writing – review & editing, Supervision, Investigation. **Miguel Pato:** Writing – review & editing, Supervision, Investigation. **Mathias Schneider:** Writing – review & editing, Investigation. **Raquel de los Reyes:** Writing – review & editing, Investigation. **Maximilian Langheinrich:** Writing – review & editing, Investigation. **Stefanie Holzwarth:** Writing – review & editing, Investigation. **Emiliano Carmona:** Writing – review & editing, Investigation. **Tobias Storch:** Writing – review & editing, Investigation. **Nicole Pinnel:** Writing – review & editing, Investigation. **Martin Habermeyer:** Writing – review & editing, Supervision, Investigation. **Raymond Kokaly:** Writing – review & editing, Supervision. **Cindy Ong:** Writing – review & editing, Supervision. **Robert O. Green:** Writing – review & editing, Supervision. **Jose Moreno:** Writing – review & editing, Supervision. **Ferran Gascon:** Writing – review & editing, Supervision. **Tobias Hank:** Data curation. **Eyal Ben-Dor:** Data curation. **Biagio Di Mauro:** Data curation. **Roberto Colombo:** Data curation. **Robert Milewski:** Data curation. **Benjamin Brede:** Data curation. **Thomas Schmid:** Data curation. **Cody Anderson:** Data curation. **Anke Schickling:** Writing – review & editing, Project administration, Funding acquisition. **Vera Krieger:** Writing – review & editing, Project administration, Funding acquisition. **Michael Bock:** Writing – review & editing, Project administration, Funding acquisition. **Laura La Porta:** Writing – review & editing, Project administration, Funding acquisition. **Sebastian Fischer:** Writing – review & editing, Project administration, Funding acquisition.

Table 3
Overview of the mission requirements and the estimated EnMAP product parameters.

Validation parameter	Sub-parameter	Estimated	Mission requirement
Radiometric uncertainty [%]	VNIR / SWIR	≤ 5.0	< 5.0
SNR	VNIR @ 495 nm & SSD 10 nm	597:1	$> 500:1$
	SWIR @ 2200 nm & SSD 10 nm	279:1	$> 150:1$
Spatially-coherent radiometric miscalibration (high-frequent)	along-track	< 1.0	–
Spatially-coherent radiometric miscalibration (low-frequent)	across-track	< 1.0	–
	across-track	< 1.0	–
Smile	VNIR @ 760 nm [% of a pixel]	4.1	< 20
	SWIR @ 2300 nm [% of a pixel]	12.5	< 20
FWHM (across-track amplitude)	VNIR @ 760 nm [% of a pixel]	6.5	–
	SWIR @ 2300 nm [% of a pixel]	10.0	–
Keystone	VNIR [% of a pixel]	7.2	< 20
	SWIR [% of a pixel]	8.1	< 20
VNIR-to-SWIR co-registration (RMSE)	x-direction [% of a pixel]	20.2	< 30
	y-direction [% of a pixel]	21.4	< 30
Absolute spatial accuracy (RMSE)	x-direction [m]	10.46	< 30
	y-direction [m]	13.49	< 30
BOA reflectance (land)	$\rho < 0.1$	< 0.01	< 0.01
	$0.1 \leq \rho < 0.3$	< 0.02	< 0.02
	$0.3 \leq \rho \leq 0.6$	< 0.04	< 0.05
Normalized water-leaving reflectance (water)	400 nm $< \lambda \leq$ 450 nm	< 0.02	< 0.04
	450 nm $< \lambda \leq$ 650 nm	< 0.02	< 0.02
	650 nm $< \lambda \leq$ 800 nm	< 0.01	< 0.01

Declaration of competing interest

The authors declare that they have no known competing financial interests or personal relationships that could have appeared to influence the work reported in this paper.

Acknowledgements

This research was supported by the EnMAP science PI project under the DLR Space Agency with funds of the Federal Ministry of Research, Technology and Space (BMFTR) on the basis of a decision by the German Bundestag (grant numbers 50EE1923 and 50EE2401). We would like to thank all involved members in carrying out the in-situ validation measurements: R. Kokaly & Todd M. Hoefen & John M Meyer & Crawford J Christopher (USGS): Black Rock Playa Zero; E. Ben-Dor & D. Heller (TAU): Amiaz Plain & Makhtesh Ramon; C. Ong (CSIRO): Pinnacles; B. Brede (GFZ) & N. Origo (NPL): Barrax; T. Schmid (CIEMAT): Camarena; R. Milewski (GFZ); Kathrin Ward (GFZ): Berlin-Tegel; T. Hank & M. Wocher (LMU): Munich-Isar; C. C. Anderson (EROS); G. Kereszturi (Massey University): Tongariro; P. Gege, I. Somlai, S. Plattner, & M. Niroumand-Jadid (DLR), M. Zeising & L. Alvarado (AWI), M. Gomes (MARE): Lake Constance; M. Brasciani & C. Giardino (CNR-IREA): Lake Trasimeno; T. Schröder (CSIRO): Lucinda Jetty Coastal Observatory (Data were sourced from Australia's Integrated Marine Observing System (IMOS) – IMOS is enabled by the National Collaborative Research Infrastructure Strategy (NCRIS); NCRIS/IMOS and CSIRO are acknowledged for funding the Lucinda Jetty Coastal Observatory); V. Brando (CNR) & the HYPERNETS project (RBINS, TARTU, SU, LOV, CNR, NPL, GFZ, CONICET): Aqua Alta Oceanographic Tower and Lampedusa; A. Dogliotti (CONICET): Rio de la Plata; D. Doxaran (LOV): Magest site; D. Vansteenwegen (VLIZ) & Q. Vanhellemont (RBINS): Oostende. Our special thanks go to the RadCalNet teams at CNES, NPL, NASA and University of Arizona for valuable additional support, in particular to A. Meygret and M. Farges (CNES).

Appendix A. Supplementary data

Supplementary data to this article can be found online at https://doi.org/10.1016/j.rse.2026.115459.

Data availability

All used EnMAP products are freely available from (DLR, 2023).

References

Alonso, Kevin, Bachmann, Martin, Burch, Kara, et al., 2019. Data products, quality and validation of the DLR Earth Sensing Imaging Spectrometer (DESIS). Sensors 19 (20), 4471. https://doi.org/10.3390/s19204471.

Asadzadeh, Saeid, Chabrillat, Sabine, 2025. Leveraging EnMAP hyperspectral data for mineral exploration: examples from different deposit types. Ore Geol. Rev. 186, 106912. https://doi.org/10.1016/j.oregeorev.2025.106912.

Bachmann, Martin, Storch, Tobias, 2023. First nighttime light spectra by satellite - by EnMAP. Remote Sens. 15 (4025), 1–25. https://doi.org/10.3390/rs15164025.

Bachmann, Martin, Alonso, Kevin, Carmona, Emiliano, et al., 2021. Analysis-ready data from hyperspectral sensors - the design of the EnMAP CARD4L-SR data product. Remote Sens. 13 (4536), 1–19. https://doi.org/10.3390/rs13224536.

Berk, Alexander, Anderson, Gail P., Acharya, Prabhat K., et al., 2006. MODTRAN5: 2006 update. In: Algorithms and Technologies for Multispectral, Hyperspectral, and Ultraspectral Imagery XII 6233 (May), pp. 508–515. https://doi.org/10.1117/12.665077.

Bialek, Agnieszka, Greenwell, Claire, Lamare, Maxim, et al., 2016. New radiometric calibration site located at Gobabeb, Namib Desert. In: *2016 IEEE International Geoscience and Remote Sensing Symposium (IGARSS)*, July, 6094–97. https://doi.org/10.1109/IGARSS.2016.7730592.

Bing, 2023. Bing Maps. In: Bing Maps. https://www.bing.com/maps?cp=52.370988%7E13.049698&lvl=11.0.

Bouvet, Marc, Thome, Kurtis, Berthelot, Béatrice, et al., 2019. RadCalNet: a radiometric calibration network for earth observing imagers operating in the visible to shortwave infrared spectral range. Remote Sens. 11 (20), 2401. https://doi.org/10.3390/rs11202401.

Bracaglia, Marco, Volpe, Gianluca, Colella, Simone, Santoleri, Rosalia, Braga, Federica, Brando, Vittorio Ernesto, 2019. Using overlapping VIIRS scenes to observe short term variations in particulate matter in the coastal environment. Remote Sens. Environ. 233 (November), 111367. https://doi.org/10.1016/j.rse.2019.111367.

Bracher, A., Soppa, M.A., Gege, P., et al., 2021. Extension of atmospheric correction polymer to hyperspectral sensors: application to HICO and first results for DESIS data. In: *2021 IEEE International Geoscience and Remote Sensing Symposium IGARSS*, July, 1237–40. https://doi.org/10.1109/IGARSS47720.2021.9553568.

Brando, Vittorio, Keen, Rex, Daniel, Paul, et al., 2010. The Lucinda Jetty Coastal Observatory's role in satellite ocean colour calibration and validation for Great Barrier Reef Coastal Waters. In: OCEANS'10 IEEE SYDNEY, pp. 1–8. https://doi.org/10.1109/OCEANSSYD.2010.5603612.

Brell, Maximilian, Guanter, Luis, Segl, Karl, et al., 2021. The EnMAP satellite –data product validation activities. In: *2021 11th Workshop on Hyperspectral Imaging and Signal Processing: Evolution in Remote Sensing (WHISPERS)*, March, 1–5. https://doi.org/10.1109/WHISPERS52202.2021.9484000.

Brell, Maximilian, Milewski, Robert, Neumann, C., et al., 2023. EnMAP Field Guide - In-Situ Measurements for Validation Purposes. *V.1.3*. GFZ. https://gfzpublic.gfz-potsdam.de/pubman/faces/ViewItemOverviewPage.jsp?itemId=item_5022656.

Bresciani, Mariano, Pinardi, Monica, Free, Gary, et al., 2020. The use of multisource optical sensors to study phytoplankton spatio-temporal variation in a shallow Turbid lake. Water 12 (1), 284. https://doi.org/10.3390/w12010284.

Carmon, Nimrod, Thompson, David R., Bohn, Niklas, et al., 2020. Uncertainty quantification for a global imaging spectroscopy surface composition investigation. Remote Sens. Environ. 251 (December), 112038. https://doi.org/10.1016/j.rse.2020.112038.

CEOS, 2023. CEOS Terms and Definition Web Page. In *Cal/Val Portal*. https://calvalportal.ceos.org/t-d_wiki.

CEOS, 2025. CEOS Analysis Ready Data Web Page. https://ceos.org/ard/.

Chabrillat, S., Ben-Dor, E., Cierniewski, J., Gomez, C., Schmid, T., van Wesemael, B., 2019. Imaging spectroscopy for soil mapping and monitoring. Surv. Geophys. 40 (3), 361–399. https://doi.org/10.1007/s10712-019-09524-0.

Chabrillat, Sabine, Guanter, Luis, Kaufmann, Hermann, et al., 2022. EnMAP science plan. GFZ Data Services. https://doi.org/10.48440/ENMAP.2022.001.

Chabrillat, Sabine, Milewski, Robert, Ward, Kathrin, et al., 2023. Monitoring Soil Properties Using EnMAP Spaceborne Imaging Spectroscopy Mission, pp. 1130–1133. https://doi.org/10.1109/IGARSS52108.2023.10282165.

Chabrillat, Sabine, Foerster, Saskia, Segl, Karl, et al., 2024. The EnMAP spaceborne imaging spectroscopy mission: initial scientific results two years after launch. Remote Sens. Environ. 315, 114379. https://doi.org/10.1016/j.rse.2024.114379.

Cogliati, S., Sarti, F., Chiarantini, L., Cosi, M., Lorusso, R., Lopinto, E., Miglietta, F., Genesio, L., Guanter, L., Damm, A., Pérez-López, S., Scheffler, D., Tagliabue, G., Panigada, C., Rascher, U., Dowling, T.P.F., Giardino, C., Colombo, R., 2021. The PRISMA imaging spectroscopy mission: overview and first performance analysis. Remote Sens. Environ. 262, 112499. https://doi.org/10.1016/j.rse.2021.112499.

Coleman, Red Willow, Thompson, David R., Brodrick, Philip G., et al., 2024. An Accuracy Assessment of the Surface Reflectance Product from the EMIT Imaging Spectrometer. Accessed July 5, 2024. https://www.authorea.com/users/751176/articles/722321-an-accuracy-assessment-of-the-surface-reflectance-product-from-the-emit-imaging-spectrometer. doi:10.22541/essoar.171328613.34483765/v1.

Czapla-Myers, Jeffrey, Thome, Kurtis, Cocilovo, Byron, McCorkel, Joel, Buchanan, John, 2008. Temporal, spectral, and spatial study of the automated vicarious calibration test site at railroad valley, Nevada. In: Proc. SPIE 7081 (August). https://doi.org/10.1117/12.795551.

Czapla-Myers, Jeffrey, Ong, Lawrence, Thome, Kurtis, McCorkel, Joel, 2016. Validation of EO-1 hyperion and advanced land imager using the radiometric calibration test site at railroad valley, Nevada. IEEE J. Select. Top. Appl. Earth Observ. Remote Sens. 9 (2).

De Vis, Pieter, Goyens, Clémence, Hunt, Samuel, Vanhellemont, Quinten, Ruddick, Kevin, Bialek, Aga, 2024. Generating hyperspectral reference measurements for surface reflectance from the LANDHYPERNET and WATERHYPERNET networks. Front. Remote Sens. 5 (May). https://doi.org/10.3389/frsen.2024.1347230.

Di Mauro, B., Cogliati, S., Bohn, N., et al., 2024. Evaluation of PRISMA products over snow in the Alps and Antarctica. Earth Space Sci. 11 (7), e2023EA003482. https://doi.org/10.1029/2023EA003482.

DLR, 2023. EOWEB GeoPortal. https://eoweb.dlr.de/egp/.

DLR, 2024. Mission - EnMAP. https://www.enmap.org/mission/.

DLR, 2025. Product Specifications and ATBDs - EnMAP. https://www.enmap.org/data_access/.

Dogliotti, Ana I., Piegari, Estefanía, Rubinstein, Lucas, Perna, Pablo, Ruddick, Kevin G., 2024. Using the automated HYPERNETS hyperspectral system for multi-mission satellite ocean colour validation in the Río de la Plata, accounting for different spatial resolutions. Front. Remote Sens. https://doi.org/10.3389/frsen.2024.1354662. Volume 5–2024.

Doxaran, David, ElKilani, Boubaker, Corizzi, Alexandre, Goyens, Clémence, 2024. Validation of satellite-derived water-leaving reflectance in contrasted French coastal waters based on HYPERNETS field measurements. Front. Remote Sens. https://doi.org/10.3389/frsen.2023.1290110. Volume 4–2023.

ESA, 2018. Sentinel-2 MSI level-2A BOA Reflectance. European Space Agency. https://doi.org/10.5270/S2_-6eb6imz.

ESA, 2023. Global Reference Image (GRI) Sentinel Online. In: Sentinel Online. https://copernicus.eu/global-reference-image.

ESA, Airbus, 2022. Copernicus DEM. European Space Agency. https://doi.org/10.5270/ESA-c5d3d65.

EUMETSAT, 2022. Recommendations for Sentinel-3 OLCI Ocean Colour Product Validations in Comparison with In Situ Measurements – Matchup Protocols.

Fischler, Martin A., Bolles, Robert C., 1981. Random sample consensus: a paradigm for model fitting with applications to image analysis and automated cartography. Commun. ACM 24 (6), 381–395. https://doi.org/10.1145/358669.358692.

FRM4SOC, 2020. Fiducial Reference Measurements for Satellite Ocean Colour (FRM4SOC). https://doi.org/10.3390/books978-3-03943-065-9.

Gao, Lianru, Du, Qian, Zhang, Bing, Yang, Wei, Wu, Yuanfeng, 2013. A comparative study on linear regression-based noise estimation for hyperspectral imagery. IEEE J. Sel. Top. Appl. Earth Obs. Remote Sens. 6 (2), 488–498. https://doi.org/10.1109/JSTARS.2012.2227245.

Gascon, Ferran, Bouzinac, Catherine, Thépaut, Olivier, et al., 2017. Copernicus sentinel-2A calibration and products validation status. Remote Sens. 9 (6), 584. https://doi.org/10.3390/rs9060584.

Giardino, C., Brando, V.E., Gege, P., et al., 2019. Imaging spectrometry of inland and coastal waters: state of the art, achievements and perspectives. Surv. Geophys. 40, 401–429. https://doi.org/10.1007/s10712-018-9476-0.

Giardino, Claudia, Bresciani, Mariano, Braga, Federica, et al., 2020. First evaluation of PRISMA level 1 data for water applications. Sensors (Basel, Switzerland) 20 (16), 4553. https://doi.org/10.3390/s20164553.

Google, 2023. Google Maps. In: Google Maps. https://www.google.de/maps/preview.

Green, R.O., Pavri, B.E., Chrien, T.G., 2003. On-orbit radiometric and spectral calibration characteristics of EO-1 hyperion derived with an underflight of AVIRIS and in situ measurements at Salar de Arizaro, Argentina. IEEE Trans. Geosci. Remote Sens. 41 (6), 1194–1203. https://doi.org/10.1109/TGRS.2003.813204.

Green, Robert O., 1998. Spectral calibration requirement for earth-looking imaging spectrometers in the solar-reflected spectrum. Appl. Opt. 37 (4), 683–690. https://doi.org/10.1364/AO.37.000683.

Guanter, Luis, Richter, Rudolf, Moreno, José, 2006. Spectral calibration of hyperspectral imagery using atmospheric absorption features. Appl. Opt. 45 (10), 2360–2370. https://doi.org/10.1364/AO.45.002360.

Guanter, Luis, Segl, Karl, Sang, Bernhard, Alonso, Luis, Kaufmann, Hermann, Moreno, Jose, 2009. Scene-based spectral calibration assessment of high spectral resolution imaging spectrometers. Opt. Express 17 (14), 11594. https://doi.org/10.1364/OE.17.011594.

Guanter, Luis, Kaufmann, Hermann, Segl, Karl, et al., 2015. The EnMAP spaceborne imaging spectroscopy mission for earth observation. Remote Sens. 7 (7), 8830–8857. https://doi.org/10.3390/rs70708830.

Guanter, Luis, Brell, Maximilian, Segl, Karl, 2022. EnMAP product validation plan EN-GFZ-PL-ValidationPlan-001 version 1.0, rev 2 march 28, 2022. GFZ.

Hank, Tobias B., Berger, Katja, Bach, Heike, et al., 2019. Spaceborne imaging spectroscopy for sustainable agriculture: contributions and challenges. Surv. Geophys. 40, 515–551. https://doi.org/10.1007/s10712-018-9492-0.

Haque, Md Obaidul, Rengarajan, Rajagopalan, Lubke, Mark, et al., 2023. *ECCOE Landsat Quarterly Calibration and Validation Report—Quarter 2, 2023*. Nos. 2023–1075. U.S. Geological Survey. https://doi.org/10.3133/ofr20231075.

Heege, T., Kiselev, V., Wettle, M., Hung, N.N., 2014. Operational multi-sensor monitoring of turbidity for the entire Mekong Delta. Int. J. Remote Sens. 35, 2910–2926. https://doi.org/10.1080/01431161.2014.890300.

Heller Pearlshtien, D., Ben-Dor, E., 2022. Calval evaluation of desis products in Amiaz plain and Makhtesh Ramon test sites, Southern Israel. In: *The International Archives of the Photogrammetry, Remote Sensing and Spatial Information Sciences* XLVI-1/W1–2021 (February), pp. 13–21. https://doi.org/10.5194/isprs-archives-XLVI-1-W1-2021-13-2022.

Helmlinger, Mark, Eastwood, Michael, Green, Robert, Thompson, David R., 2016. Solar-similar near-infra-red suppressed ‘Blue’ calibration source. In: *2016* IEEE Aerospace Conference, March, 1–11. https://doi.org/10.1109/AERO.2016.7500714.

IOCCG, 2019. *Ocean Optics and Biogeochemistry Protocols for Satellite Ocean Colour Sensor Validation, Volume 3.0: Protocols for Satellite Ocean Colour Data Validation: In Situ Optical Radiometry*. Edited by G. Zibordi, K. J. Voss, B. C. Johnson, and J. L. Mueller. 3.0. IOCCG Protocol Series. International Ocean-Colour Coordinating Group (IOCCG). https://doi.org/10.25607/OBP-691.

Justice, C., Belward, A., Morisette, J., Lewis, P., Privette, J., Baret, F., 2000. Developments in the ‘validation’ of satellite sensor products for the study of the land surface. Int. J. Remote Sens. 21 (17), 3383–3390. https://doi.org/10.1080/014311600750020000.

Kaufmann, Hermann, Sang, Bernhard, Storch, Tobias, et al., 2015. Environmental Mapping and Analysis Program – a German Hyperspectral Mission. In: Chap. 7 in *Optical Payloads for Space Missions*. John Wiley & Sons, Ltd. https://doi.org/10.1002/9781118945179.ch7.

Kiselev, Viacheslav, Bulgarelli, Barbara, Heege, Thomas, 2015. Sensor independent adjacency correction algorithm for coastal and inland water systems. Remote Sens. Environ. 157 (February), 85–95. https://doi.org/10.1016/j.rse.2014.07.025. Special Issue: Remote Sensing of Inland Waters.

Kokhanovsky, Alexander, Chevrollier, Lou-Anne, Wehrlé, Adrien, Segl, Karl, Chabrillat, Sabine, 2026. A simple analytical model for the reflection function of flat glacier ice surfaces and its application for optical remote sensing of glaciers. J. Quant. Spectrosc. Radiat. Transf. 351, 109717. https://doi.org/10.1016/j.jqsrt.2025.109717.

Laffoy, S., Vountas, M., Mei, L., Bösch, H., 2025. First results of the XBAER aerosol optical depth algorithm with EnMAP data. EGUsphere 2025, 1–19. https://doi.org/10.5194/egusphere-2025-1282.

Loew, Alexander, Bell, William, Brocca, Luca, et al., 2017. Validation practices for satellite-based earth observation data across communities. Rev. Geophys. 55 (3), 779–817. https://doi.org/10.1002/2017RG000562.

Reyes, Raquel de los, Langheinrich, Maximilian, Schwind, Peter, et al., 2020. PACO: Python-based atmospheric correction. Sensors 20 (5), 1428. https://doi.org/10.3390/s20051428.

Miura, Tomoaki, Smith, Charlotte Z., Yoshioka, Hiroki, 2021. Validation and analysis of terra and aqua MODIS, and SNPP VIIRS vegetation indices under zero vegetation conditions: a case study using railroad valley playa. Remote Sens. Environ. 257, 112344. https://doi.org/10.1016/j.rse.2021.112344.

Mouroulis, Pantazis, Green, Robert O., Chrien, Thomas G., 2000. Design of pushbroom imaging spectrometers for optimum recovery of spectroscopic and spatial information. Appl. Opt. 39 (13), 2210–2220. https://doi.org/10.1364/AO.39.002210.

Mustafa, Wan Azani, Yazid, Haniza, Khairunizam, Wan, et al., 2019. Image enhancement based on discrete cosine transforms (DCT) and discrete wavelet transform (DWT): a review. IOP Conf. Ser.: Mater. Sci. Eng. 557 (1), 012027. https://doi.org/10.1088/1757-899X/557/1/012027.

Neville, Robert A., Sun, Lixin, Staenz, Karl, 2003. Detection of spectral line curvature in imaging spectrometer data. In: Algorithms and Technologies for Multispectral, Hyperspectral, and Ultraspectral Imagery IX 5093 (September), pp. 144–154. https://doi.org/10.1117/12.487342.

Niro, Fabrizio, Goryl, Philippe, Dransfeld, Steffen, et al., 2021. European Space Agency (ESA) calibration/validation strategy for optical land-imaging satellites and pathway towards interoperability. Remote Sens. 13 (15), 3003. https://doi.org/10.3390/rs13153003.

Oktem, R., Ponomarenko, N.N., 2007. Image filtering based on discrete cosine transform. Telecommun. Radio Eng. 66 (18). https://doi.org/10.1615/TelecomRadEng.v66.i18.70.

Ong, C., Caccetta, M., Lau, I.C., Ong, L., Middleton, E., 2017. Compositional characterisation of the pinnacles vicarious calibration site. In: *2017* IEEE International Geoscience and Remote Sensing Symposium (IGARSS), July, 3059–62. https://doi.org/10.1109/IGARSS.2017.8127644.

Pogrebnyak, Oleksiy, Lukin, Vladimir V., 2012. Wiener discrete cosine transform-based image filtering. J. Electron. Imag. 21.

Roger, J., Irakulis-Loitxate, I., Valverde, A., Gorroño, J., Chabrillat, S., Brell, M., Guanter, L., 2024. High-resolution methane mapping with the EnMAP satellite imaging spectroscopy mission. IEEE Trans. Geosci. Remote Sens. 62, 1–12. https://doi.org/10.1109/TGRS.2024.3352403.

Ruddick, K., Beck, M., Bialek, A., Brando, V., et al., 2022. WATERHYPERNET: automated in situ measurements of hyperspectral water reflectance for satellite validation … And More. In: Proceedings “Oceans from Space”, pp. 68–69. https://doi.org/10.57648/OceansFromSpaceV-2022-PROCEEDING.

Ruddick, Kevin George, Bialek, Agnieszka, Brando, Vittorio Ernesto, Dogliotti, Ana Ines, Doxaran, David, Goyens, Clemence, 2025. Editorial: optical radiometry and satellite validation. Front. Remote Sens. https://doi.org/10.3389/frsen.2025.1585494. Volume 6–2025.

Scheffler, Daniel, 2023. AROSICS: An Automated and Robust Open-Source Image Co-Registration Software for Multi-Sensor Satellite Data. V. v1.9.0. Zenodo, released May. https://doi.org/10.5281/zenodo.7897030.

Scheffler, Daniel, Hollstein, André, Diedrich, Hannes, Segl, Karl, Hostert, Patrick, 2017. AROSICS: an automated and robust open-source image co-registration software for multi-sensor satellite data. Remote Sens. 9 (7), 676. https://doi.org/10.3390/rs9070676.

Schroeder, Thomas, Schaale, Michael, Lovell, Jennifer, Blondeau-Patissier, David, 2022. An ensemble neural network atmospheric correction for sentinel-3 OLCI over coastal waters providing inherent model uncertainty estimation and sensor noise propagation. Remote Sens. Environ. 270 (March), 112848. https://doi.org/10.1016/j.rse.2021.112848.

Segl, Karl, Guanter, Luis, Rogass, Christian, Kuester, Theres, Roessner, Sigrid, Kaufmann, Hermann, Sang, Bernhard, Mogulsky, Valery, Hofer, Stefan, 2012. EeteS—the EnMAP end-to-end simulation tool. IEEE J. Select. Top. Appl. Earth Observ. Remote Sens. 5 (2), 522–530. https://doi.org/10.1109/JSTARS.2012.2188994.

Slater, P.N., Biggar, S.F., Holm, R.G., et al., 1987. Reflectance- and radiance-based methods for the in-flight absolute calibration of multispectral sensors. Remote Sens. Environ. 22 (1), 11–37. https://doi.org/10.1016/0034-4257(87)90026-5.

Slater, Phlip N., Biggar, Stuart F., Thome, Kurtis J., Gellman, David I., Spyak, Paul R., 1996. Vicarious radiometric calibrations of EOS sensors. J. Atmos. Ocean. Technol. 13 (2), 349–359. https://doi.org/10.1175/1520-0426(1996)013<0349:VRCOES>2.0.CO;2.

Soppa, M.A., Dinh, D.A., Silva, B., Steinmetz, F., Alvarado, L., Bracher, A., 2022. Intercomparison of Desis, Sentinel-2 (MSI) and Sentinel-3 (OLCI) data for water colour applications. In: *The International Archives of the Photogrammetry, Remote Sensing and Spatial Information Sciences* XLVI-1-W1–2021 (February), pp. 69–72. https://doi.org/10.5194/isprs-archives-XLVI-1-W1-2021-69-2022.

Soppa, Mariana A., Brell, Maximilian, Chabrillat, Sabine, et al., 2024. Full mission evaluation of EnMAP water leaving reflectance products using three atmospheric correction processors. Opt. Express 32 (16), 28215–28230. https://doi.org/10.1364/OE.523813.

Storch, Tobias, Honold, Hans-Peter, Chabrillat, Sabine, et al., 2023. The EnMAP imaging spectroscopy mission towards operations. Remote Sens. Environ. 294 (August), 113632. https://doi.org/10.1016/j.rse.2023.113632.

Tahersima, Mohammad H., Thome, Kurtis, Wenny, Brian N., et al., 2025. The characterization of the Railroad Valley Playa test site using the DESIS imaging spectrometer from the Space Station orbit. Remote Sens. 17 (3). https://doi.org/10.3390/rs17030396.

Thome, K.J., Helder, D.L., Aaron, D., Dewald, J.D., 2004. Landsat-5 TM and landsat-7 ETM+ absolute radiometric calibration using the reflectance-based method. IEEE Trans. Geosci. Remote Sens. 42 (12), 2777–2785. https://doi.org/10.1109/TGRS.2004.839085.

Thompson, D.R., Braverman, A., Brodrick, P.G., Candela, A., Carmon, N., Clark, R.N., Connelly, D., Green, R.O., Kokaly, R.F., Li, L., Mahowald, N., Miller, R.L., Okin, G.S., Painter, T.H., Swayze, G.A., Turmon, M., Susilouto, J., Wettergreen, D.S., 2020. Quantifying uncertainty for remote spectroscopy of surface composition. Remote Sens. Environ. 247, 111898. https://doi.org/10.1016/j.rse.2020.111898.

Thompson, David R., Green, Robert O., Bradley, Christine, et al., 2024. On-orbit calibration and performance of the EMIT imaging spectrometer. Remote Sens. Environ. 303 (March), 113986. https://doi.org/10.1016/j.rse.2023.113986.

Thompson, David, Thompson, David R., Green, Robert O., et al., 2023. On-orbit calibration and performance of the EMIT imaging spectrometer. ESS Open Arch. Eprints 290 (July), essoar.168988432. https://doi.org/10.22541/essoar.168988432.29040205/v1.

Turpie, Kevin R., Casey, Kimberly A., Crawford, Christopher J., et al., 2023. Calibration and validation for the Surface Biology and Geology (SBG) Mission Concept: Recommendations for a multi-sensor system for imaging spectroscopy and thermal imagery. J. Geophys. Res. Biogeosci. 128 (9), e2023JG007452. https://doi.org/10.1029/2023JG007452.

Vabson, Viktor, Ansko, Ilmar, Duong, Kim, et al., 2024. Complete characterization of ocean color radiometers. Front. Remote Sens. 5, 1320454.

Vansteenwegen, Dieter, Ruddick, Kevin, Cattrijsse, André, Vanhellemont, Quinten, Beck, Matthew, 2019. The Pan-and-tilt hyperspectral radiometer system (PANTHYR) for autonomous satellite validation measurements—prototype design and testing. Remote Sens. 11 (11), 1360.

Vermote, Eric F., Kotchenova, Svetlana, 2008. Atmospheric correction for the monitoring of land surfaces. J. Geophys. Res. Atmos. 113 (D23). https://doi.org/10.1029/2007JD009662.

Vis, De, Pieter, Agnieszka Bialek, Sinclair, Morven, 2023. Initial sample of HYPERNETS hyperspectral surface reflectance measurements for satellite validation from the gobabeb site in Namibia. Zenodo. https://doi.org/10.5281/ZENODO.8039303.

Wang, Zhou, Bovik, A.C., Sheikh, H.R., Simoncelli, E.P., 2004. Image quality assessment: from error visibility to structural similarity. IEEE Trans. Image Process. 13 (4), 600–612. https://doi.org/10.1109/TIP.2003.819861.